

Analyst

Accepted Manuscript



This is an *Accepted Manuscript*, which has been through the Royal Society of Chemistry peer review process and has been accepted for publication.

Accepted Manuscripts are published online shortly after acceptance, before technical editing, formatting and proof reading. Using this free service, authors can make their results available to the community, in citable form, before we publish the edited article. We will replace this *Accepted Manuscript* with the edited and formatted *Advance Article* as soon as it is available.

You can find more information about *Accepted Manuscripts* in the [Information for Authors](#).

Please note that technical editing may introduce minor changes to the text and/or graphics, which may alter content. The journal's standard [Terms & Conditions](#) and the [Ethical guidelines](#) still apply. In no event shall the Royal Society of Chemistry be held responsible for any errors or omissions in this *Accepted Manuscript* or any consequences arising from the use of any information it contains.

Gold nanorod-based localized surface plasmon resonance platform for the detection of environmentally toxic metal ions

Subramaniam Jayabal^{a*}, Alagarsamy Pandikumar^a, Hong Ngee Lim^b, Ramasamy Ramaraj^{a,c}, Tong Sun^d, Nay Ming Huang^{a*}

^aLow Dimensional Materials Research Centre, Department of Physics, Faculty of Science, University of Malaya, 50603 Kuala Lumpur, Malaysia.

^bDepartment of Chemistry, Faculty of Science & Functional Device Laboratory, Institute of Advanced Technology, Universiti Putra Malaysia, 43400 UPM Serdang, Selangor, Malaysia.

^cSchool of Chemistry, Centre for Photoelectrochemistry, Madurai Kamaraj University, Madurai-625021, India.

^dSchool of Engineering and Mathematical Sciences, City University London, London EC1V 0HB, United Kingdom.

*Corresponding authors E-mail: jayabal84@gmail.com (Subramaniam Jayabal), huangnayming@um.edu.my (Nay Ming Huang).

Abstract

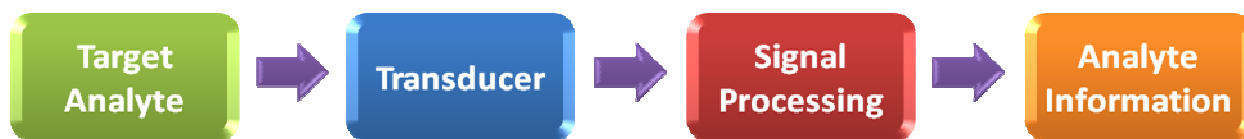
Gold nanorods (Au NRs) are elongated nanoparticles with unique optical properties which depend on their shape anisometry. The Au NR-based longitudinal localized surface plasmon resonance (longitudinal LSPR) band is very sensitive to the surrounding local environment and upon the addition of target analytes, the interaction between the analytes and the surface of the Au NRs leads to a change in the longitudinal LSPR band. This makes it possible to devise Au NR probes with application potential to the detection of toxic metal ions with an improved limit of detection, response time, and selectivity for the fabrication of sensing devices. The effective surface modification of Au NRs helps to improve their selectivity and sensitivity toward the detection of toxic metal ions. In this review, we discuss different methods for the preparation of surface modified Au NRs for the detection of toxic metal ions based on the LSPR band of the Au NRs and the types of interactions between the surface of Au NRs and

1
2
3 metal ions. We summarize the work that has been done on Au NR-based longitudinal LSPR
4
5 detection of environmentally toxic metal ions, sensing mechanisms, and the current progress on
6
7 the various modified Au NR-based longitudinal LSPR sensors for toxic metal ions. Finally, we
8
9 discuss the applications of Au NR-based longitudinal LSPR sensors to real sample analysis and
10
11 some of the future challenges facing longitudinal LSPR -based sensors for the detection of toxic
12
13 metal ions toward commercial devices.
14
15
16

17 18 **1. Introduction**

19
20 Gold nanorods (Au NRs) are elongated nanoparticles with unique optical properties,
21
22 which depend on their size and aspect ratio (their length-to-breadth ratio).¹⁻⁷ Au NRs possess
23
24 two principal plasmon absorption bands: a transverse localized surface plasmon resonance
25
26 (transverse LSPR) band located in the visible region around 520 nm and a longitudinal localized
27
28 surface plasmon resonance (longitudinal LSPR) band located at a longer wavelength region
29
30 which can be tuned by varying the aspect ratio of the Au NRs from the visible to the near-IR
31
32 region.¹⁻⁹ The unique properties of Au NRs find applications in the fields of imaging, therapy
33
34 and sensing.⁹⁻¹² A sensor is a device that measures or detects a physical parameter and converts
35
36 it into a signal, which is subsequently read by an observer or instrument.¹³ Fig. 1 shows a
37
38 schematic representation of three main components of a sensor system, the analyte (target
39
40 sample), transducer (platform/probe), and signal-processing device.¹⁴ An optical sensor involves
41
42 the addition of the target analyte of our interest to a sensor probe or transducer, which gives a
43
44 detectable signal which provide the analyte information.¹⁵ Optical sensors have several
45
46 advantages compared to other sensing methods, such as unmatched sensitivity, multianalyte
47
48
49
50
51
52
53
54
55
56
57
58
59
60

1
2
3 detection, non-invasiveness, and low toxicity.¹⁶ Optical sensor research is mainly driven by the
4
5 needs of clinical chemistry, biotechnology and environmental chemistry.^{14,16}
6
7



8
9
10
11
12
13
14 Fig. 1 Schematic representation of main components of sensor system.
15

16
17 In recent years, the development of new materials is essential for the advancement of
18 optical sensors. The nanomaterials-based optical sensors have extensive applications with
19 improved sensitivity, and selectivity, lower production costs, reduced power consumption and
20 improved stability.¹⁷ The unique optical properties of nanoscale materials make them ideal
21 candidate for new generation sensing devices for optical sensor applications.¹⁸ An efficient
22 sensor has a better response time, signal-to-noise (S/N) ratio, selectivity, and limits of detection
23 (LOD).¹⁹ Therefore, designing an efficient sensor depends on the properties of novel materials
24 that improve the potential sensing performance.¹⁸ Particularly, Au NRs have unique optical
25 properties that give them great utility in the designing of novel sensors for the detection of target
26 analytes.
27
28
29
30
31
32
33
34
35
36
37
38
39

40 The most common optical sensors are absorption- and luminescence-based sensors.¹⁴ For
41 Au NR-based longitudinal LSPR sensor, the absorption-based sensors are commonly developed
42 by using the longitudinal LSPR band of Au NRs.¹⁻³ Absorption-based colorimetric sensors have
43 been developed based on the shift observed in the longitudinal LSPR band of Au NRs due to the
44 i) change in the interparticle distance of the NRs and (ii) change in the refractive index of the
45 local surrounding environment. Colorimetric sensors are extremely attractive because target
46 analytes can be simply detected with the naked eye in the presence of interferences.^{19,20}
47
48
49
50
51
52
53
54
55
56
57
58
59
60

1
2
3
4
5
6
7
8
9
10
11
12
13
14
15
16
17
18
19
20
21
22
23
24
25
26
27
28
29
30
31
32
33
34
35
36
37
38
39
40
41
42
43
44
45
46
47
48
49
50
51
52
53
54
55
56
57
58
59
60

Colorimetric sensors based on nanomaterials have attracted much attention in recent years due to their simplicity, rapidity and novelty.^{19,21–23} Therefore, Au NR-based longitudinal LSPR sensor is effectively used as a principle for optical detection of target analytes. For the development of selective and sensitive detection of specific target analytes, Au NRs are usually modified with functional group biomolecules or functionalized silica-based materials, which interact selectively with the target analytes of interest, making them detectable using the longitudinal LSPR band of the modified Au NRs.^{3,4}

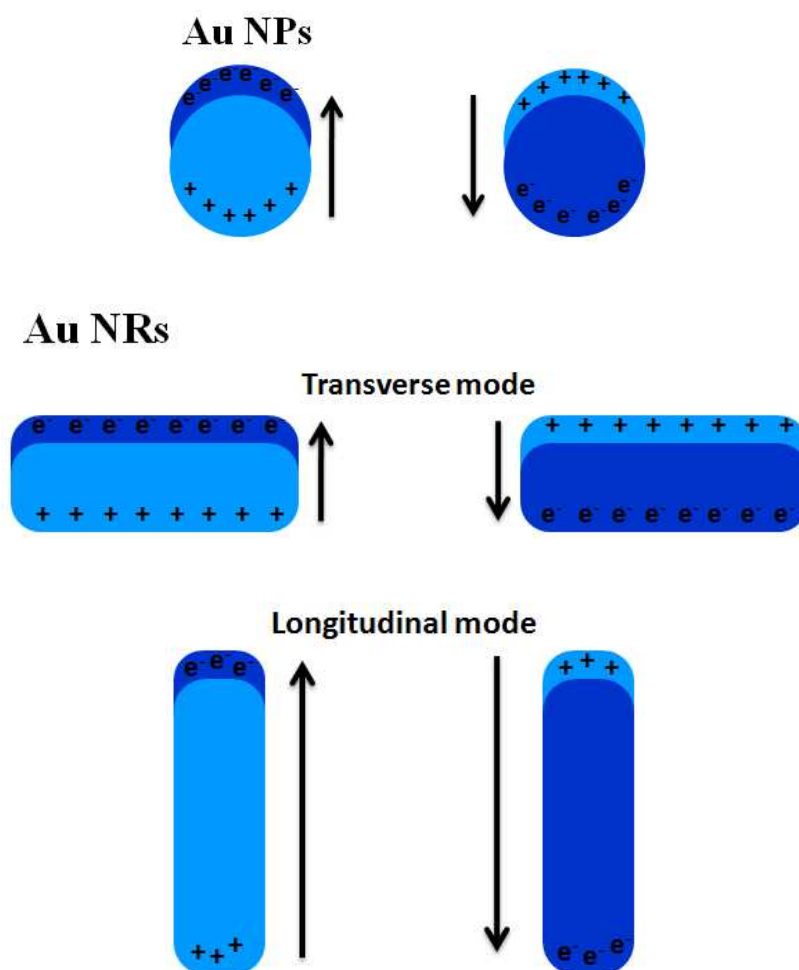
The term toxic metal ions refers to any metallic elements that has a relatively high density and are poisonous even at low concentration.²⁴ The toxic metals ions are not biodegradable and hence they commonly exist in air, water and soil.^{13,20,25–32} For this reason, safety limits or maximum levels for the toxic metal ions present in drinking water have been fixed by World Health Organization (WHO) and Environmental Protection Agency (EPA) from all over the world.³³ The toxic metal ions have a tendency to form complexes with biological ligands of containing nitrogen, sulfur, and oxygen which produces changes in molecular structure of proteins, with the result that the breaking of hydrogen bonds or inhibition of enzymes.^{25–32} These interactions may lead to toxicological and carcinogenic effects. In particular, the metal ions such as Hg²⁺, Pb²⁺, and As³⁺ ions affect the central nervous system; Cu²⁺, Cd²⁺, Hg²⁺, and Pb²⁺ ions affect the kidneys and liver; and Ni²⁺, Cu²⁺, Cd²⁺, and Cr³⁺ ions affect the skin, bones, and teeth.^{25–32} Therefore, the developments of simple methods to detect traces of toxic metal ions in environmental and living systems are extremely relevant for controlling the pollution of metal ions. In recent years, the Au NRs have been used for the detection of metal ions by utilizing their longitudinal LSPR/interparticle distance dependent optical properties and high extinction coefficients.^{34,35}

1
2
3 In this review article, we summarize the use of a surface-modified Au NR-based
4 longitudinal LSPR sensor as an effective platform for the detection of metal ions and also discuss
5 the different surface modification methods for Au NRs, Au NR-based longitudinal LSPR
6 detection methods, and the different interaction between the surface of the NRs and metal ions.
7
8 Finally, we discuss the practical applications to real sample analysis and some key future
9 challenges to improve the sensitivity and selectivity of the proposed sensor. We hope and expect
10 that this review will be useful to newcomers and give direction to the field of Au NR-based
11 longitudinal LSPR sensors.
12
13
14
15
16
17
18
19
20
21

22 **2. Properties of Au NRs**

23
24
25
26 The optical properties of metallic NPs usually arise from localized surface plasmon
27 resonance, which occurs, when the incoming electromagnetic radiation interacts with the
28 conduction band free electrons. This induces the coherent oscillation of free electrons, which
29 gives rise to a strong absorption band in the visible-NIR region of the electromagnetic spectrum
30 depending on the size and shape of the particles, and also shows remarkable bright colors which
31 could not be observed in the bulk materials.³⁶⁻³⁹ When spherical Au NPs are exposed to
32 incoming electromagnetic radiation, the free electrons present in the conduction band are excited,
33 and the columbic electrostatic attraction of the nuclei will restore these free electrons to their
34 original positions, resulting in coherent oscillations of the free electrons when the frequency of
35 the light oscillations matches that of the incident light (Fig. 2).³⁶⁻³⁹ The position of the SPR band
36 strongly depends on the size and shape of the nanoparticles. When the shape of the nanoparticles
37 changes, the surface geometry also changes, with a shift in the local electric field density on the
38 particle surface upon the irradiation of light, which finally causes a change in the frequency of
39
40
41
42
43
44
45
46
47
48
49
50
51
52
53
54
55
56
57
58
59
60

1
2
3 the oscillations.³⁶ In particular, for Au NRs, the SPR absorption splits into two bands
4 corresponding to the oscillation of the free electrons along (longitudinal mode) and perpendicular
5 (transverse mode) to the long axis of the NRs (Fig. 2). The transverse LSPR band (transverse
6 mode) shows absorption at around 520 nm, while the longitudinal LSPR band (longitudinal
7 mode) usually shows absorption at a longer wavelength and strongly depends on the aspect ratio
8 of the NRs (Fig. 3).¹⁻³ If the aspect ratio of the Au NRs is increased, the wavelength of the
9 longitudinal LSPR band is shifted to the longer wavelength and the color of the NR solution also
10 changes.⁴⁰



54
55
56 Fig. 2 Schematic representation of SPR excitation for Au NPs and Au NRs.

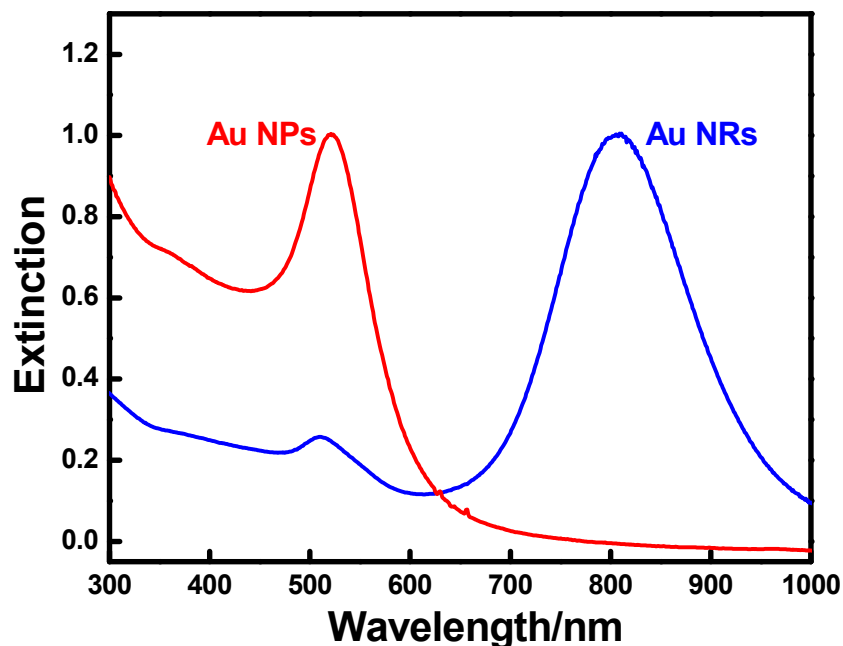


Fig. 3 Extinction spectra of spherical Au NPs and Au NRs.

The presence of the longitudinal LSPR band in Au NRs is extremely sensitive to any change in the refractive index of the solvent and the presence of a capping agent or shell layer on the surface of the NRs.¹ The excellent sensitivity of the longitudinal LSPR band is also due to the interparticle distance between the Au NRs. The presence of a strong longitudinal LSPR absorption intensity in Au NRs gives rise to improved sensitivity in the field of optical sensors.^{3,34} Therefore, the longitudinal LSPR band is very sensitive to the local surrounding environment, when compared to the transverse LSPR band, as well as the SPR band of spherical Au NPs. This is due to the presence of the following two effects:

- i) Strong light scattering and
- ii) Large electric field enhancement

The longitudinal LSPR band strongly depends on the scattering and absorption of light, along with the electric field intensity at the surface of the NRs.¹⁻³ The scattering and absorption

1
2
3 components are strongly depends on the surface properties of Au NRs.^{1–3,41,42} The position of the
4 longitudinal LSPR band is easily measured using a conventional UV–visible spectrophotometer
5 and appears as a band in the longer wavelengths (600–1100 nm), which depends on the aspect
6 ratio of the NRs. The Au NRs scatter light very efficiently compared to spherical Au NPs, and
7 are also involved in the measurement of the UV–visible spectrum (extinction spectrum).⁴³ The
8 extinction spectrum is the combination of the absorption and scattering.^{44,45} The enhancement of
9 the electric field is due to the surface plasmon oscillations generated with the incoming light.^{3,36}
10 The local electric field density strongly depends on the geometry of the metallic NPs.^{3,36} For Au
11 NRs, the high intensity of the longitudinal LSPR band is due to strong surface plasmon
12 oscillations in longitudinal mode compared to the surface plasmon oscillations of transverse
13 LSPR band and spherical Au NPs, which leads to an large enhancement of the electric field at
14 the NR surface.^{3,46,47} In particular, Au NRs have a higher electric field generated at the tips and
15 edges of the NRs.^{3,46,47} Because of the presence of a strong scattering effect and large electric
16 field enhancement upon the irradiation of light, Au NRs can be effectively used in applications in
17 the fields of chemical sensors, surface-enhanced Raman scattering (SERS), and biological
18 imaging.^{1,3,9}

3. Preparation of Au NRs

19
20 The preparation of Au NRs with a high yield and uniform shape control is necessary to
21 ensure their unique optical properties for various applications. The preparation of Au NRs with a
22 100 % yield of NRs is a difficult task.⁴⁸ Therefore, the preparation of Au NRs with a higher yield
23 and uniform shape has been an emerging field in recent years. For the preparation of Au NRs,
24 there are two general methods, i.e., bottom-up and top-down methods.³ In the bottom-up
25
26
27
28
29
30
31
32
33
34
35
36
37
38
39
40
41
42
43
44
45
46
47
48
49
50
51
52
53
54
55
56
57
58
59
60

1
2
3 methods, Au NRs are prepared by the growth of particles starting from metal atoms, which are
4 obtained from Au precursors. These include the wet chemical method,^{48–52} electrochemical
5 method,⁵³ sonochemical method,⁵⁴ photochemical method,⁵⁵ solvothermal method,⁵⁶ and
6 microwave-assisted method.⁵⁷ In these methods, Au NRs are prepared by the reduction of Au
7 salts using various reducing agents such as sodium borohydride, ascorbic acid, and small Au
8 clusters, in the presence of different external agents. In the top-down methods, Au NRs are
9 prepared by a combination of different physical lithography techniques and deposition of
10 Au.^{3,58,59} However, the top-down methods are generally time consuming and highly expensive.³
11
12 The preparations of Au NRs by various methods and their growth mechanisms have already been
13 discussed in many reviews by different groups such as Huang et al.,¹ Perez-Juste et al.,² Chen et
14 al.,³ Vigderman et al.³⁴

15
16
17
18
19
20
21
22
23
24
25
26
27
28
29
30
31
32
33
34
35
36
37
38
39
40
41
42
43
44
45
46
47
48
49
50
51
52
53
54
55
56
57
58
59
60

The most common method used for the preparation of Au NRs is the seed-mediated growth method developed by El-Sayed et al.⁴⁸ and Murphy et al.⁴⁹ because of its simplicity, high NR yield, uniform size control, and easy surface modification. In the typical seed-mediated growth method developed by El-Sayed et al.,⁴⁸ a seed solution of Au nanoparticles with a size of <4 nm is initially prepared by reducing chloroauric acid with borohydride in an aqueous cetyltrimethylammonium bromide (CTAB) solution. Then, the growth solution is obtained by the reduction of Au³⁺ ions into Au⁺ ions with the aid of a mild reducing agent (ascorbic acid) in an aqueous CTAB solution containing AgNO₃. Finally, a certain amount of the seed solution is added to the growth solution for the formation of Au NRs. The aspect ratio of Au NRs is controlled by varying the amount of AgNO₃. The NR yield using this method is >99%. Here, the CTA–Br–Ag⁺ complex acts as a face-specific capping agent that selectively binds with the higher-energy (110) facets of the Au nanocrystals, which slows down the growth on these facets.

1
2
3 Thus, Au atoms will be mainly deposited onto the (100) facets, which leads to the longitudinal
4 growth of the NR-like shape.^{3,51} Using this seed-mediated growth method in the presence of Ag⁺
5 ions gives a single-crystalline Au NR structure.⁶⁰ Murphy et al.,⁴⁹ prepared Au NRs by the seed-
6 mediated growth method in the absence of Ag⁺ ions. In the absence of Ag⁺ ions, the prepared Au
7 NR solution contains a mixture of rods, spheres, and plates, and the pure NRs are finally
8 separated using centrifugation. Using this seed-mediated growth method in the absence of Ag⁺
9 ions gives a pentahedrally-twinned Au NR structure.⁶⁰ In recent years, many researchers have
10 focused on the synthesis of Au NRs using different methods with high yields and uniformity.
11
12
13
14
15
16
17
18
19
20
21
22

23 **4. Chemical modification of Au NRs**

24
25
26 The direct use of Au NRs for sensors has not been widely pursued because of the CTAB
27 bilayers capped on the surface of the Au NRs which limit the applications in the fields of
28 nanotechnology and biology.^{2,3,7,61} The large amount of CTAB dispersed in Au NR solution will
29 interfere with some biomolecules and also has significant cytotoxicity.⁶¹⁻⁶³ The unbound CTAB
30 layers present in the Au NR solution are toxic to the cultivated cells.⁶¹ Therefore, the excess
31 CTAB present in the Au NR solution is removed by centrifugation. After centrifugation, the
32 obtained Au NRs are unstable, mainly because of the desorption of CTAB molecules from the
33 Au NR surface.^{7,62,64} Therefore, the surface of the Au NRs should be modified with specific
34 functional group biomolecules or polymer-based materials to enhance the applications of Au
35 NRs in the fields of nanotechnology and biology.⁶⁵⁻⁷³ The surface functionalization of Au NRs
36 will provide a stable platform for an optical sensor system with improved sensitivity and
37 selectivity. For the effective detection of metal ions with more advantages, the Au NRs are
38 generally modified with a specific functionalized group that interacts selectively with the target
39
40
41
42
43
44
45
46
47
48
49
50
51
52
53
54
55
56
57
58
59
60

1
2
3 analytes of analytical interest. The surface functionalization of Au NRs by suitable functional
4 groups has attracted considerable attention because of the improved stability, functionality, and
5 application potential.^{68,69} In recent years, surface modified Au NRs have constituted an emerging
6 field, and modified Au NRs have been used for optical sensor and biological applications.^{3,9,34}
7
8
9

10
11
12 The modification of Au NRs are done by two approaches: non-covalent interaction,
13 involving the physical adsorption of the functional groups on the surface of NRs and covalent
14 interaction, involving chemical binding of the functional groups on the surface of the NRs.⁷⁴⁻⁷⁷
15

16
17 The surface of the Au NRs is generally modified using different methods, which include ligand
18 exchange, layer-by-layer (LbL), and surface coating (Table 1).^{40,69,72} Fig. 4 shows a schematic
19 representation of the different methods for the modification of Au NRs. In the ligand exchange
20 method, some biomolecules and thiol compounds are used to modify the CTAB bilayer, which
21 form a strong bond with the surface of the Au NRs.^{78,79} Takahashi et al.⁷⁸ reported a method for
22 the preparation of modified Au NRs using phosphatidylcholine, which reduces the cytotoxicity
23 of the Au NRs for practical applications. Another report by Dai et al.⁷⁹ developed a method for
24 the efficient replacement of the CTAB bilayer surfactants on Au NRs using the bifunctional thiol
25 ligand 11-mercaptoundecanoic acid inside an ionic exchange resin, which resulted in a good
26 solubility and stability against the aggregation of Au NRs in organic solvents. Layer-by-layer
27 (LbL) approaches involve the effective coating of the NR surface without removing the CTAB
28 bilayer. The LbL approach involves the sequential deposition of anionic and cationic
29 polyelectrolytes with oppositely charged surfaces through electrostatic self-assembly.⁶⁹ The first
30 step involves the adsorption of an anionic polyelectrolyte due to the presence of cationic
31 surfactant CTAB on the surface of the Au NRs. Gole et al.⁸⁰ reported a method for the
32 preparation of polyelectrolyte-coated Au NRs by the LbL technique using poly(sodium-4-
33
34
35
36
37
38
39
40
41
42
43
44
45
46
47
48
49
50
51
52
53
54
55
56
57
58
59
60

1
2
3 styrenesulfonate) and poly(diallyldimethylammonium chloride) as electrolytes. Takahashi et al.⁸¹
4
5 also developed a method for the preparation of modified Au NRs with bovine serum albumin and
6
7 polyethylenimine by using the LbL technique and showed cellular uptake activity. Although this
8
9 method makes it simple to prepare a uniform coating thickness using cationic and anionic
10
11 polyelectrolytes, the bonding between the polymer and the surface of the Au NRs is noncovalent,
12
13 which leads to low stability, and the polyelectrolytes limit the surface functionality of the Au
14
15 NRs.⁸² Surface coating of Au NRs by silica- or polymer-based materials reduces their
16
17 interparticle aggregation and thereby enhances their stability.² In addition, the silica-based
18
19 surface-coated Au NRs possess a large pore size, high surface area, good stability, and
20
21 biocompatibility.^{83–85} When compared to other modification methods, silica-based modified Au
22
23 NRs has been widely used because of its simple modification process and has demonstrated
24
25 effective applications in sensor fields. Sendroiu et al.⁸⁶ reported a method for coating a thin shell
26
27 of silica over Au NRs using 3-mercaptopropyl trimethoxysilane and sodium silicate for the
28
29 functionalization of amine modified single-stranded DNA to improve the sensitivity of surface
30
31 plasmon resonance imaging measurements on DNA microarrays. Another study by Wang et al.⁸⁷
32
33 prepared mesoporous silica-coated Au NRs using tetraethoxysilane in a NaOH medium for the
34
35 sensitive colorimetric detection of ascorbic acid induced by silver overcoating.
36
37
38
39
40
41
42

Different modification methods	Surface modifying molecules/compounds/materials	Ref.
Ligand exchange	Biomolecules, and thiol compounds.	78,79
Layer-by-layer (LbL)	Anionic, and cationic polyelectrolytes	80,81
Surface coating	Polymer, and silica materials	86,87

43
44
45
46
47
48
49
50
51
52
53
54
55
56 Table 1 Summary of different of surface modification methods.
57
58
59
60

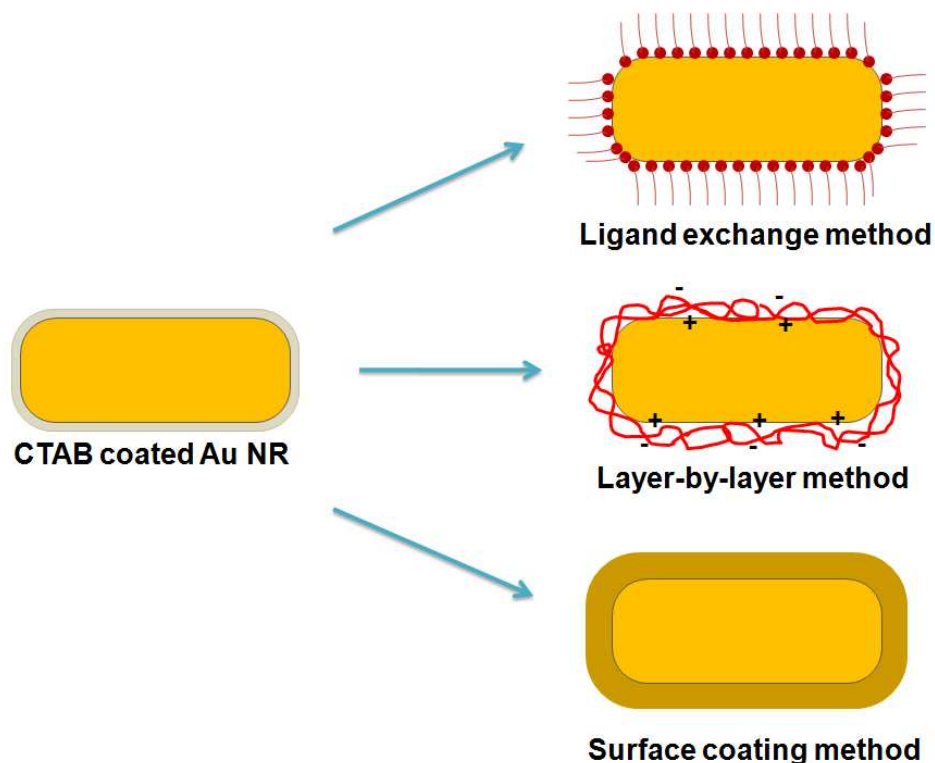


Fig. 4 Schematic representation of different methods for modification of Au NRs.

The surface modified Au NRs showed a significant change in the wavelength of the longitudinal LSPR band, along with a small change in the transverse LSPR band of the Au NRs. These changes are due to the i) change in the local refractive index of the medium surrounding the NRs after modification and ii) the change in the aspect ratio of the NRs after modification.^{83,88} The surface functionalized Au NRs will act as both a recognition element for the analyte receptor and a transducer for signal processing, thereby simplifying the sensor design, with improves sensitivity and selectivity. Fig. 5 shows a pictorial diagram of the various applications of surface-modified Au NRs.^{9,11,12,87,89}

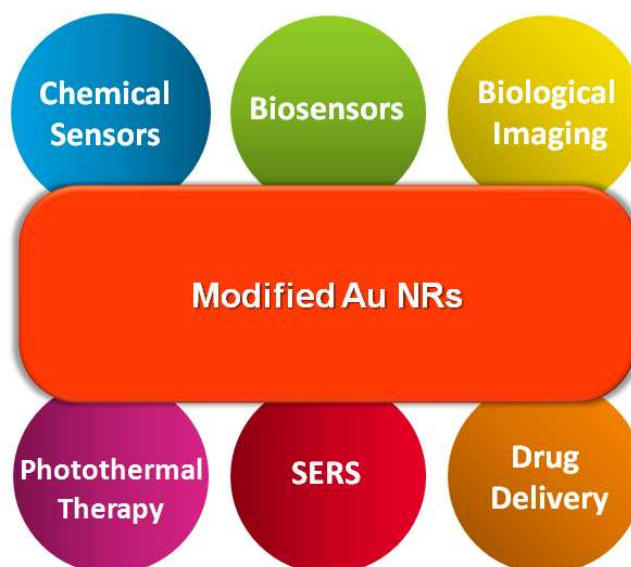


Fig. 5 Pictorial diagram of various applications of surface-modified Au NRs.

5. Au NR-based LSPR detection of metal ions

5.1. Different detection methods

5.1.1. Absorption-based detection

UV–visible (absorption)-based sensing has generally been used for the detection of toxic metal ions using Au NR-based probes. The absorption-based sensor mechanism is the measurement of the shift in the wavelength of the longitudinal LSPR band during the interaction of metal ions with the surface of a Au NR probe due to change in the dielectric constant of the surrounding medium and also changes in the interparticle distance of the NRs after formation of the assembly or aggregation.^{3,34} This type of absorption-based detection method using Au NRs for the sensing of metal ions exhibits a much higher sensitivity than spherical Au NPs.⁹⁰

The surface modified Au NR-based sensor systems show good sensitivity and selectivity toward the target analytes.^{87,90} The Au NRs chemically modified with a specific functional group will preconcentrate the target analytes around the surface of the NRs and produce an effective

1
2
3 adsorption of analytes on the surface of the Au NRs. Fig. 6 shows a schematic representation of
4
5 an absorption-based detection system using modified Au NR probes. The interaction between the
6
7 surface modified Au NRs and target analytes alters the physicochemical properties of the
8
9 transducer Au NRs, such as the longitudinal LSPR absorption, scattering, and local electric field
10
11 density. Finally these changes produce a detectable response signal. The interaction of metal ions
12
13 with the surface of modified Au NRs will change the dielectric constant of the surrounding
14
15 material, which induces changes in the frequency of the oscillation due to the change in the
16
17 electron density on the surface of the NRs. As a result, a considerable shift is observed in the
18
19 longitudinal LSPR absorption band of the Au NRs. The shift in the wavelength of the
20
21 longitudinal LSPR absorption band to a shorter or longer wavelength depends upon the type of
22
23 the interaction of the metal ions with the surface of the Au NR probe, as discussed in later sub-
24
25 sections. Therefore, Au NR-based probe/transducer is used as an effective platform for the
26
27 selective and sensitive detection of toxic metal ions. The absorption-based detection of various
28
29 metal ions using Au NR-based probes is tabulated in Table 2.
30
31
32
33
34
35
36
37
38
39
40
41
42
43
44
45
46
47
48
49
50
51
52
53
54
55
56
57
58
59
60

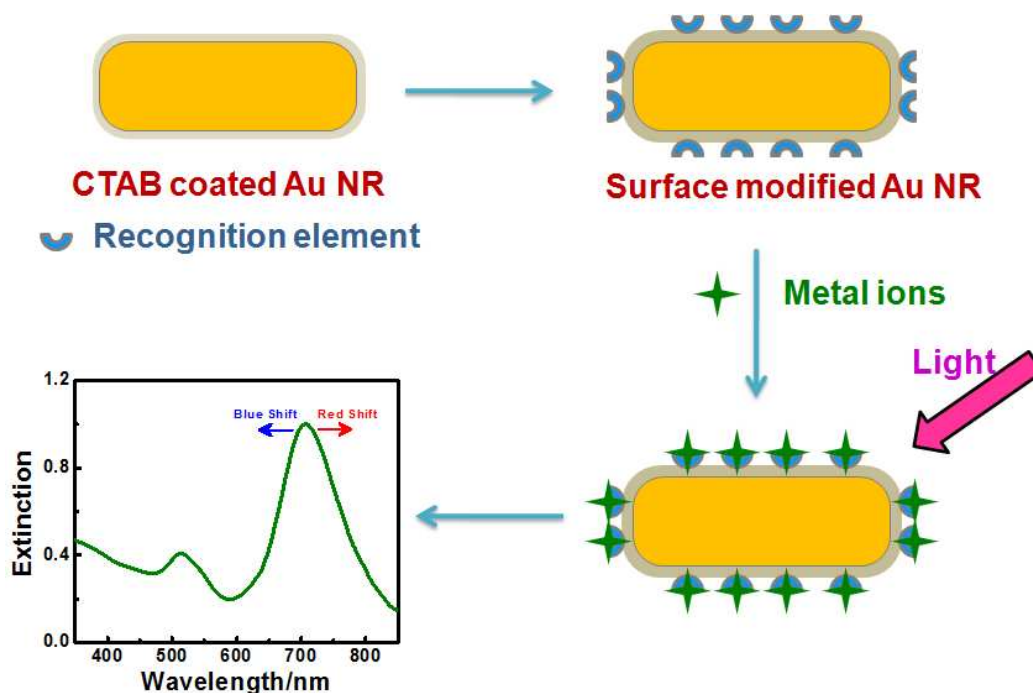


Fig. 6 Schematic representation of absorption-based detection system using modified Au NRs.

Absorption-based colorimetric detection method has attracted great interest because of their unique advantages such as simplicity, novelty, low cost and lack of analytical instrumentation requirements.^{21,22,91-95} The colorimetric detection of metal ions using Au NR-based systems is a proof-of-concept for the development of a sensor system, since it is easily visible to the naked eye in the detection of Hg^{2+} ions with high sensitivity and selectivity. The color of the Au NRs depends on their aspect ratio and the dielectric constant of the surrounding medium, which includes the stabilizing agent, functionalization, shell coating on the surface of the NRs.¹⁻³ By using the color dependent properties, Au NR-based sensor systems can be effectively used for colorimetric detection of toxic metal ions. The color change during the aggregation (or assembly or morphology change) of Au NR-based probes provides a convenient analytical platform for the absorption-based colorimetric detection of any specific target analyte.

The aggregation of the Au NRs produces a decrease in the interparticle distance of the NRs, which results changes in the plasmon coupling and leads to a color change, even at very low concentrations.¹⁸ The sensitivity and selectivity of Au NR-based sensors depend on their aspect ratio and density of NRs, as well as the nature of the target analytes.

Placido et al.⁹⁶ reported a colorimetric sensing of Hg^{2+} ions using pyrazole-derived amino ligand functionalized Au NRs. Upon the addition of 30 ppb Hg^{2+} ions, the color of the solution is changed with a red shift in the longitudinal LSPR band of the Au NR probes, as shown in Fig. 7.

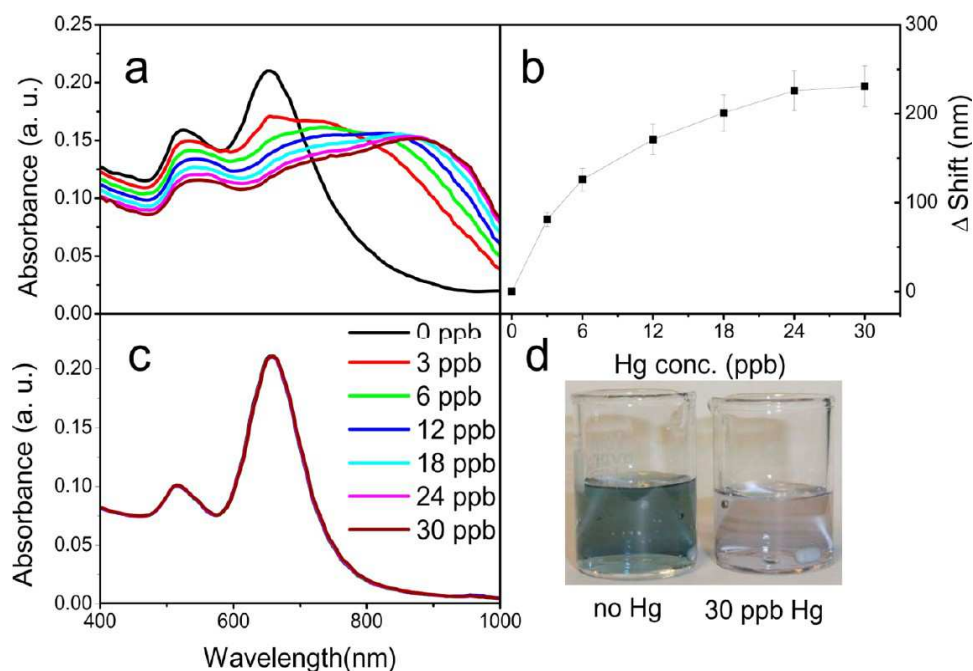


Fig. 7 UV-vis absorption spectra of (a) "PyL treated" Au NRs upon addition of increasing concentration of Hg^{2+} ions (from 0 to 30 ppb), (b) shift in longitudinal LSPR band with increasing concentration of Hg^{2+} ions, (c) "as prepared" Au NRs with increasing concentration of Hg^{2+} ions, and (d) photograph of beakers containing Au NR solution before and after addition of Hg^{2+} ions. Reproduced with permission from ref. 96 Copyright 2013 The American Chemical Society.

In an another study, Jayabal et al.⁹⁷ developed a selective colorimetric sensor for the detection of Hg^{2+} ions using Au NRs embedded in a silicate sol–gel matrix. The longitudinal LSPR absorption band of the Au NRs in the silicate sol–gel showed a blue shift with a significant decrease in the absorption intensity upon 1 μM increases in the concentration of Hg^{2+} ions. Fig. 8 presents a plot of the shift in the LSPR band maximum (λ_{LSPR}) of the Au NRs in the silicate sol–gel against the concentration of Hg^{2+} ions, which shows two linear lines corresponding to the lower (1 μM to 10 μM) and higher (10 μM to 20 μM) concentrations of Hg^{2+} ions. The addition of a 10 μM concentration of Hg^{2+} ions to the Au NRs in the silicate sol–gel solution led to a color change, and this trend correlates with the two linear lines at the lower and higher concentrations observed in the plot (Fig. 8). The colorimetric sensing of various metal ions using Au NR-based probes is tabulated in Table 2.

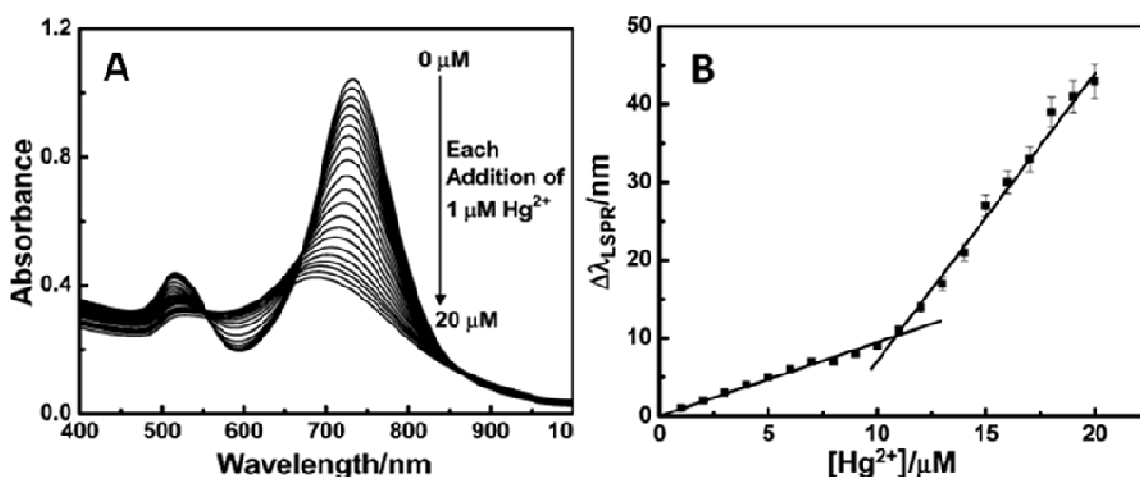


Fig. 8 (A) Absorption spectral changes observed for Au–TPDT NRs upon each 1 μM addition of Hg^{2+} ions to solution. (B) Plot of shift in the longitudinal LSPR band maximum ($\Delta\lambda_{\text{LSPR}}$) of Au–TPDT NRs against concentrations of Hg^{2+} ions. Reproduced with permission from ref. 97 Copyright 2014 The Royal Society of Chemistry.

Table 2. Summary of reports in literature on Au NR-based probes for metal ion sensing

Probe	Detection method	Metal ions	Type of Interaction	Linear Range	LOD	Ref.
PyL-Au NRs	Absorption and colorimetric	Hg ²⁺	End-to-end formation	0 – 6 ppb	11 pM (3 ppt)	96
TPDT Silicate-Au NRs	Absorption and colorimetric	Hg ²⁺	Morphology change and AuHg amalgamation	1 μM – 7 μM	0.317 μM	97
Au NRs	Absorption	Fe ²⁺	End-to-end formation	-	-	113
Cys-Au NRs	Absorption and colorimetric	Cu ²⁺	End-to-end formation	1–100 μM	0.34 μM	114
Cys-Au NRs	Absorption	Pb ²⁺	Side-by-side assembly and aggregation	0.1 nM – 1 nM	0.1 nM	115
DTT-Au NRs	Absorption	Hg ²⁺	Aggregation	1–50 nM	0.42 nM	116
ssDNA-Au NRs	Absorption and colorimetric	Pb ²⁺	Aggregation	5 nM – 1 μM	3 nM	117
Au NRs	Absorption	Hg ²⁺	AuHg amalgam formation and morphology changes	1.98×10 ⁻¹² – 3.11×10 ⁻⁸ g/L	2.43 fM (6.6×10 ⁻¹³ g/L)	118
Au NRs	Absorption	Hg ²⁺	AuHg amalgam formation and morphology changes	2.0 μg/L – 0.58 mg/L	3.68 nM (1 μg/L)	119
Silica-CN-Au NRs	Colorimetric	Hg ²⁺	AuHg amalgam formation	50 nM – 5 μM	5.4 nM	120
Au NRs	Absorption	Hg ²⁺	AuHg amalgam formation	-	-	121
Au NRs	Absorption and colorimetric	Cu ²⁺	Catalytic etching	5 nM – 500 mM	1.6 nM	122
Au NRs	Colorimetric	Cu ²⁺	Catalytic etching	10 – 300 nM	4.96 nM	123

Au NRs	Colorimetric	Pb ²⁺	Etching and Pd-Au alloy formation	10 nM – 1 μM	4.3 nM	124
Au NRs	Colorimetric	Cu ²⁺	Catalytic etching	7 – 50 nM	2.7 nM	125
Au NRs	Absorption	Fe ³⁺	Agglomeration	-	0.25 μM (100 ppb)	126
MS-Au NRs	Absorption and colorimetric	Hg ²⁺	Redox-mediated inner particle interaction	1 nM – 1 mM	0.79 nM	90
Polyamine-capped Au NRs	Absorption	Cu ²⁺	Chelation	1 μM – 5 mM	0.24 μM	127
Au NRs	Absorption	Fe ³⁺ , Hg ²⁺ , Cu ²⁺ , and Ag ⁺	Changes of nanostructure and composition	-	-	128

5.1.2. Other Detection Methods

There are various methods reported for the detection of toxic metal ions using Au NRs as a probe, including fluorescence resonance energy transfer (FRET),^{98,99} plasmon resonance energy transfer (PRET),¹⁰⁰ plasmonic circular dichroism,¹⁰¹ and surface-enhanced Raman scattering (SERS)¹⁰² techniques and the standard techniques for the detection of trace metal ions such as atomic absorption spectroscopy¹⁰³ (AAS), inductively coupled plasma-mass spectrometry¹⁰⁴ (ICP-MS), and electrochemical¹⁰⁵ methods. Although these techniques offer sufficient sensitivity towards the detection of toxic metal ions, each method has its own advantages and drawbacks. Moreover, these methods are time-consuming, require complex instrumentation, trained professionals, and complicated sample preparation processes. The Au NR-based longitudinal LSPR sensor provides simplicity, a short time delay, cost-effectiveness, good selectivity and sensitivity. Hence, the detection of toxic metal ions using the Au NR-based

1
2
3 longitudinal LSPR method is more suitable for a sensor platform for evaluating low
4
5 concentrations of toxic metal ions.
6
7

8 9 **5.2. Interactions involved in the detection of metal ions using Au NRs**

10
11 The Au NRs prepared by seed-mediated growth method in the absence of Ag^+ ions have
12 a five-fold twinned NR structure, and in the presence of Ag^+ ions, a single-crystalline NR
13 structure is obtained.^{48,49,60} The five-fold twinned Au NRs have a side-facet of (110) and edge-
14 facet of (111), and single-crystalline NRs have side-facets of (110) or (100) and edge-facets of
15 (111) or (100), which depend on the cross-sections of the NRs.^{106,107} The surface energy of the
16 (110) crystallographic facets is higher than that of the (100) and (111) facets.^{108,109} The side facet
17 (110) is thickly covered with a CTAB bilayer whereas the end-facets (111) and (100) are less
18 thickly covered due to the lower surface energies of the (111) and (100) facets compared to the
19 (110) facet. Thus, the CTAB bilayer predominately binds with the conventionally less stable
20 (110) facet and produces more stability. The presence of side-facets (110) or (100) and edge-
21 facets (111) or (100) is beneficial for surface modification and also induces the specific
22 interaction with the surface of the Au NRs and metal ions, where as such specific interaction is
23 not possible in the Au spherical nanoparticles which consist of only (111) and (100) surface
24 facets.¹¹⁰ Fig. 9 shows the different structural models of the Au NRs, with their specific planes.
25
26 The interaction between metal ion and the surface of the Au NRs probe gives various types of
27 interaction includes end-to-end assembly formation, side-by-side assembly formation,
28 aggregation-based formation, etc.
29
30
31
32
33
34
35
36
37
38
39
40
41
42
43
44
45
46
47
48
49
50
51
52
53
54
55
56
57
58
59
60

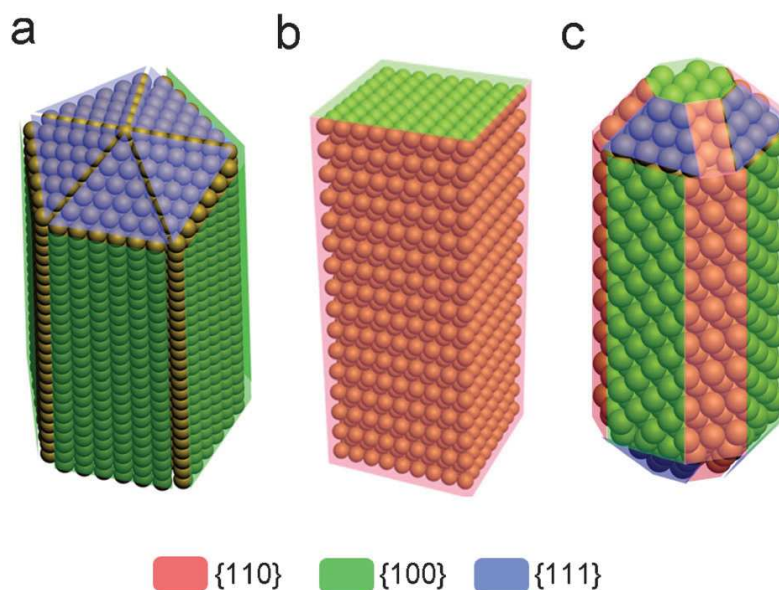
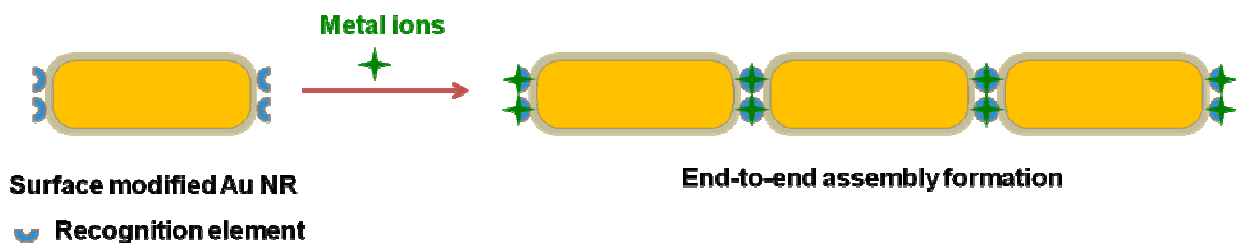


Fig. 9 Structural models of Au NRs. (a) Five-fold twinned NR, (b) single-crystalline NR with rectangular cross-section and (c) single-crystalline NR with octagonal cross-section. Reproduced with permission from ref. 98 Copyright 2014 The Royal Society of Chemistry.

5.2.1. End-to-end assembly formation

In the end-to-end assembly interaction, the metal ions preferentially bind with the (111) or (100) facets present in the edges of the modified Au NRs through specific interactions or binding leading to chain/wire-like formations. The end-to-end assembly formation in the Au NRs with the specific interaction of the target analytes generally causes a red shift in the longitudinal LSPR band, with no significant shift in the transverse LSPR band. A schematic representation of the end-to-end assembly formation in the sensing of metal ions using modified Au NRs is shown in Fig. 10.



1
2
3 Fig. 10 Schematic representation of end-to-end assembly formation
4
5

6 The red shift observed in the longitudinal LSPR band is due to the decrease in the
7 internanorod distance upon end-to-end assembly formation.^{98,109–111} The strength of the
8 longitudinal plasmon coupling increases with decreasing the internanorod distance, which results
9 a red shift in the longitudinal LSPR band for the end-to-end assembly formation. When the
10 number of NRs increases in this assembly formation, the strength of the longitudinal plasmon
11 also increases, which results larger red shift in the longitudinal LSPR band.¹¹² This inter-nanorod
12 plasmon coupling mechanism can be qualitatively correlated with the exciton coupling theory by
13 treating the NR plasmon oscillation as an exciton. In the exciton coupling theory,¹¹² the excited-
14 state plasmon modes of the monomer split into either in-phase (symmetric) or out-of-phase
15 (antisymmetric) modes, leading to the formation of a lower energy bonding plasmon mode or a
16 higher energy antibonding plasmon mode, respectively (Fig. 11). If the incident polarization is
17 along the longitudinal axis of the end-to-end NR dimer, the excited state plasmon mode is
18 favored in the in-phase transition at lower energy because of the attractive dipole moments of the
19 two NRs in the longitudinal polarization configuration, which produces a red shift in the
20 longitudinal LSPR band. In contrast, the out-of-phase transition at a higher energy is not favored
21 because of the cancellation of the two dipole moments in the longitudinal polarization
22 configuration (Fig. 11). Because of the attractive dipole interaction at a lower energy, the end-to-
23 end assembly interaction is more sensitive than the side-by-side assembly interaction.
24
25
26
27
28
29
30
31
32
33
34
35
36
37
38
39
40
41
42
43
44
45
46
47
48
49
50
51
52
53
54
55
56
57
58
59
60

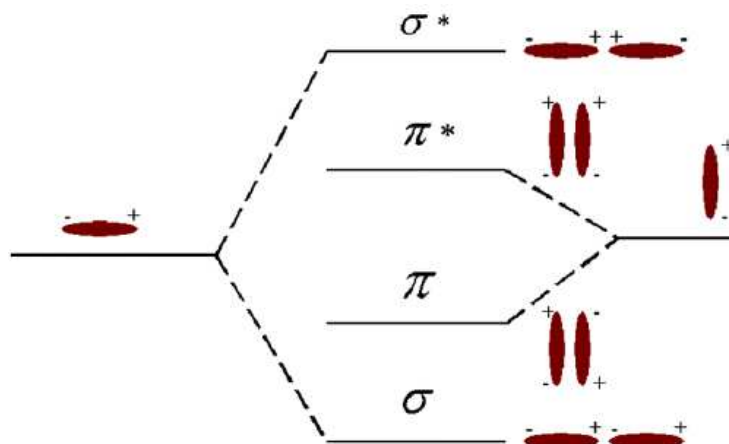


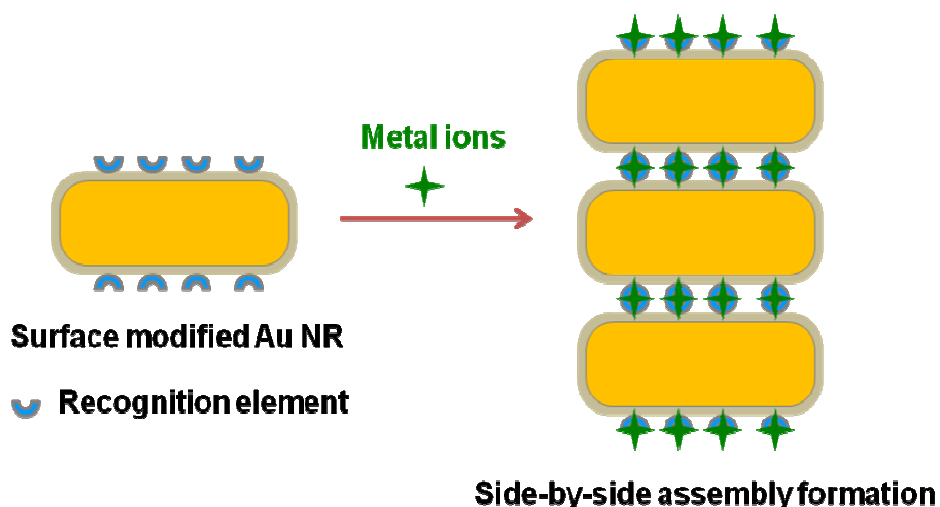
Fig. 11 Exciton theory picture of the nature of the coupled longitudinal plasmon excitation in NRs dimers: electromagnetic analogy to molecular orbital theory. Reproduced with permission from ref. 112 Copyright 2006 The American Chemical Society.

Placido et al.⁹⁶ reported the preparation of pyrazole-derived amino ligand functionalized Au NRs for the detection of Hg^{2+} ions, where an increase in the concentration of the Hg^{2+} ions causes a gradual red shift and broadening of the longitudinal LSPR band due to the formation of end-to-end assembly (Fig. 7). The Hg^{2+} ions interact preferably at their tips with the specific topology of the ligand-modified Au NRs. The LOD obtained by using this method was 11 pM (3 ppt), which is lower than the EPA standard for the maximum allowable level (10 nM) of mercury in drinking water. Selvakannan et al.¹¹³ prepared thiol-terminated terpyridine functionalized Au NRs which selectively bound Fe^{2+} ions through an end-to-end one-dimensional self-assembly formation with decreases in the intensity and a red shift in the longitudinal LSPR band due to the thiol groups binding the (111) end facets of the NRs, which selectively bound the edges of the tips of the NRs to induce the end-to-end assembly formation. Liu et al.¹¹⁴ developed a probe for the selective and sensitive detection of Cu^{2+} ions using cysteine-modified Au NRs. The CTAB preferentially binds with the side faces of the Au NRs compared to the end faces and thus hinders the binding of cysteine to the side faces of the Au NRs. The detection of Cu^{2+} ions is

1
2
3 based on the a red shift in the longitudinal LSPR band due to the strong coordination of Cu^{2+}
4 ions with cysteine, which results in a stable Cys–Cu–Cys complex through the end-to-end
5 assembly of the Au NRs along with a color change. The LOD obtained using this method was
6 0.34 μM , which is lower than the EPA standard for the maximum allowable level (20 μM) of
7 copper in drinking water. This method was successfully applied to the determination of the Cu^{2+}
8 ions in tap water, lake water and river water samples.
9
10
11
12
13
14
15
16
17

18 5.2.2. Side-by-side assembly formation

19
20 In the side-by-side assembly interaction, the metal ions specifically bind with the sides of
21 the NRs through specific interactions or binding, while the surface of the NRs is already
22 modified with the specific functional group by utilizing the (110) side and (111) end facets
23 present on the surface of the NRs. The assembly of Au NRs by side-by-side interaction using a
24 specific interaction with a target analyte generally causes a blue shift in the longitudinal LSPR
25 band and a red shift in the transverse LSPR band. A schematic representation of the side-by-side
26 assembly interaction in the sensing of metal ions using modified Au NRs is shown in Fig. 12.
27
28
29
30
31
32
33
34
35
36



55 Fig. 12 Schematic representation of side-by-side assembly formation

1
2
3
4
5
6
7
8
9
10
11
12
13
14
15
16
17
18
19
20
21
22
23
24
25
26
27
28
29
30
31
32
33
34
35
36
37
38
39
40
41
42
43
44
45

The blue shift observed in the longitudinal LSPR band is due to the decrease in the internanorod distance upon side-by-side assembly formation.^{98,112} The strength of the longitudinal plasmon coupling increases with decreasing internanorod distance, which results a blue shift in the longitudinal LSPR band for the side-by-side assembly formation. When the number of interacting NRs increases in this assembly formation, the strength of the longitudinal plasmon coupling also increases, which results a larger blue shift in the longitudinal LSPR band.¹¹² On the basis of the exciton coupling theory,¹¹² if the incident polarization is along the longitudinal axis of a side-by-side NR dimer (Fig. 11), the excited state plasmon mode is favored in the out-of-phase transition at higher energy because of the attractive dipole moments of the two NRs in the longitudinal polarization configuration, which produces a blue shift in the longitudinal LSPR band. In contrast, the in-phase transition at lower energy is not favored because of the cancellation of two dipole moments in the longitudinal polarization configuration. If the incident polarization is along the transverse axis of a side-by-side NR dimer (Fig. 11), the excited state plasmon mode is favored in the in-phase transition at lower energy because of the attractive dipole moments in the transverse polarization arrangement, which results a red shift in the transverse LSPR band. In contrast, the out-of-phase transition at higher energy is not favored because of the cancellation of the two dipole moments in the transverse polarization arrangement.

46
47
48
49
50
51
52
53
54
55
56
57
58
59
60

Cai et al.¹¹⁵ prepared cysteine-functionalized Au NRs, which acted as probes for the detection of Pb^{2+} ions by the formation of side-by-side assembly interaction with a small blue shift and decrease in the intensity of the longitudinal LSPR band along with a slight change in the transverse LSPR peak after the addition of Pb^{2+} ions. The interaction with cysteine-functionalized Au NRs involves their long sides with the Pb^{2+} ions, due to the specific topology

of cysteine. The LOD obtained using this method was 0.1 nM, which is lower than the EPA standard for the maximum allowable level (75 nM) of lead in drinking water. This method was successfully applied to the determination of Pb^{2+} ions in real tap water samples.

5.2.3. Aggregation-based formation

The aggregation of Au NRs generally leads to a color change in the solution. The formation of aggregates affects the plasmonic properties of the Au NRs and also changes their absorption and scattering effects. A schematic representation of the formation of aggregates in the sensing of metal ions using modified Au NRs is shown in Fig. 13.

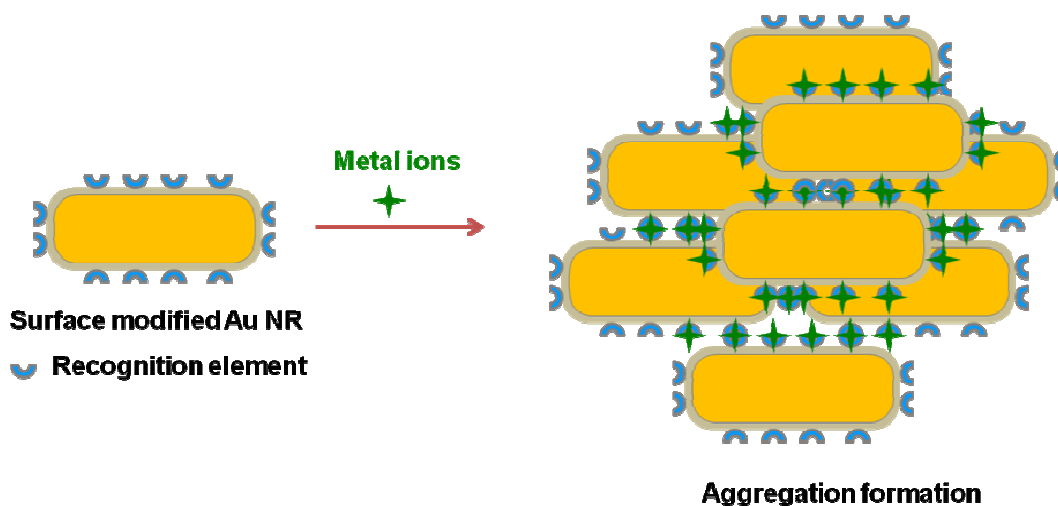


Fig. 13 Schematic representation of aggregation-based formation

Bi et al.¹¹⁶ developed a simple method for the detection of Hg^{2+} ions using Au NRs in the presence of dithiothreitol. In this method, Au NRs are aggregated in the presence of dithiothreitol. However, after the addition of Hg^{2+} ions, a strong coordination of Hg^{2+} ions with thiol groups present in the dithiothreitol results in a stable Hg–S bond formation with a color change and also inhibits the aggregation of the Au NRs. The LOD obtained using this method was 0.42 nM. This method was successfully applied to the determination of Hg^{2+} ions in real

1
2
3 water samples. Chen et al.¹¹⁷ developed a probe for the selective and sensitive label-free
4
5 colorimetric method for detection of Pb^{2+} ions using Au NRs based on the conformational switch
6
7 from single-stranded DNA to G-quadruplex. The detection of Pb^{2+} ions involves a decrease in
8
9 the intensity of the longitudinal LSPR band with a blue shift due to the strong electrostatic
10
11 interaction of Pb^{2+} ions with single-stranded DNA, which results in the formation of a G-
12
13 quadruplex through the aggregation of the Au NRs in a side-by-side manner, along with a color
14
15 change. The LOD obtained using this method was 3 nM. This method was successfully applied
16
17 to the determination of Pb^{2+} ions in real tap water samples.
18
19
20
21
22

23 **5.2.4. Amalgam-based formation**

24
25 The amalgam-based formation sensing mechanism has attracted great interest particularly
26
27 for the detection of Hg^{2+} ions. Rex et al.¹¹⁸ reported the use of Au NRs in the presence of an
28
29 excess amount of NaBH_4 for the detection of Hg^{2+} ions with high sensitivity. Upon the addition
30
31 of Hg^{2+} ions to the Au NR solution in the presence of excess NaBH_4 , morphology of the Au NRs
32
33 is changed to spherical particles through an amalgamation process between the Au and Hg (Fig.
34
35 14). This is also supported by the blue shift observed in the absorption spectra of the Au NRs
36
37 upon each addition of Hg^{2+} ions (Fig. 14). The active sites of the Au NRs are at tips and edges,
38
39 which result in the formation of amalgams more efficiently on the tips and edges of the NRs by
40
41 decreasing their aspect ratio. Moreover, the shielding effect also restricts the amalgam formation
42
43 of Hg on the lateral walls of the NRs, which leads to a change in the morphology of the Au NRs
44
45 to spherical particles. The Fig. 14(A) shows a schematic diagram of the amalgam between the
46
47 Hg and Au NRs. The TEM image (Fig. 14(B)) shows that the morphology of the Au NRs is
48
49 changed to spherical particles upon increasing the concentration of Hg^{2+} ions in the Au NR
50
51 solution containing NaBH_4 , and corresponding EDS analysis also shows the increasing Hg
52
53
54
55
56
57
58
59
60

content. The LOD obtained using this method was 2.43 fM ($6.6 \times 10^{-13} \text{ g L}^{-1}$). This method was successfully applied to the determination of Hg^{2+} ions in real tap water samples.

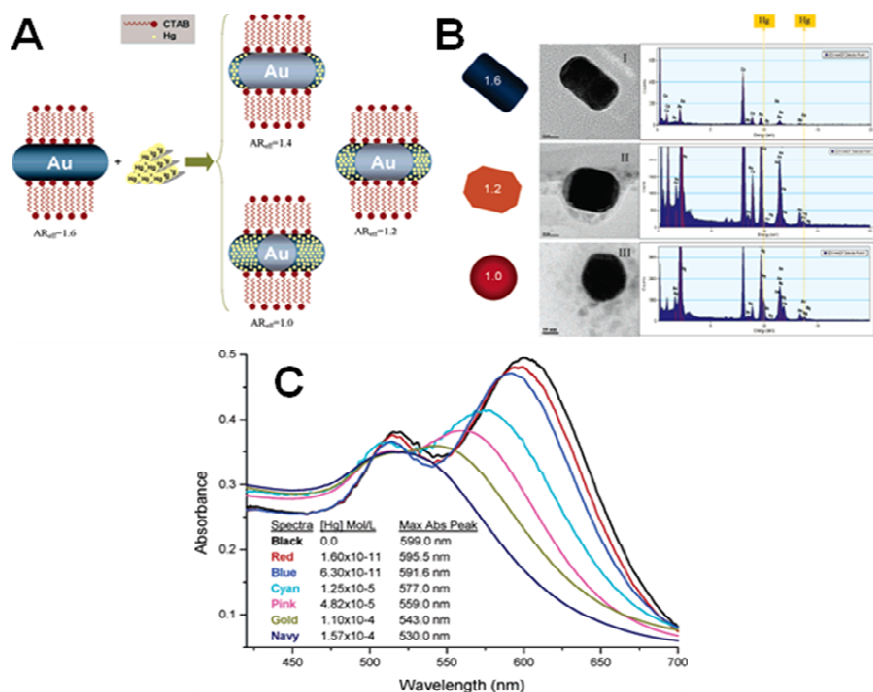


Fig. 14 (A) Schematic diagram showing amalgamation of Hg with Au NRs. (B) TEM and EDS analysis results of Au NRs in the absence of Hg^{2+} ions (I) and in the presence of Hg^{2+} ions at concentrations of $1.25 \times 10^{-5} \text{ M}$ (II) and $1.57 \times 10^{-4} \text{ M}$ (III). All solutions were prepared in $1.67 \times 10^{-3} \text{ mol/L NaBH}_4$. (C) Absorption spectra of different concentrations of Hg^{2+} ions. Reproduced with permission from ref. 118 Copyright 2006 The American Chemical Society.

Jayabal et al.⁹⁷ reported the preparation and application of an amine-functionalized silicate sol-gel matrix embedded in Au NRs for the selective detection of Hg^{2+} ions through the formation of AuHg amalgam. Upon the addition of the Hg^{2+} ions to the amine-functionalized silicate-coated Au NRs, the Hg^{2+} ions were selectively adsorbed on the tips and edges of the NR structures, which resulted in the formation of an amalgam, with a change in the morphology of the NRs to spherical nanoparticles. Here, Au NRs were partially oxidized to Au(I) by the Hg^{2+} ions; simultaneously Hg^{2+} was reduced to $\text{Hg}(0)$, which formed a layer coating the Au NRs and

1
2
3 led to a change in the morphology of the NR structure. The LOD obtained using this method was
4
5 0.317 μM . This method was successfully applied to the determination of Hg^{2+} ions in real water
6
7 samples. Chemnasiri et al.¹¹⁹ developed a Au NR-based mercury sensor using Au NRs on a
8
9 functionalized glass substrate. The longitudinal LSPR band of the Au NRs experienced a blue
10
11 shift after the addition of Hg^{2+} ions in the presence of NaBH_4 due to the formation of an
12
13 amalgam. The LOD obtained using this method was 3.68 nM ($1.0 \mu\text{g L}^{-1}$). Anand et al.¹²⁰
14
15 developed a sensitive, selective, and label free optical method for the detection of Hg^{2+} ions
16
17 using cyano ligand-functionalized Au NRs in the presence of ascorbic acid. Poly(2-
18
19 aminobenzonitrile) was used for the functionalization of Au NRs. The sensing of Hg^{2+} ions is
20
21 understood by the preconcentration of Hg^{2+} ions on the surface of cyano ligand-functionalized
22
23 Au NRs through the interaction of the $-\text{CN}$ groups with Hg^{2+} ions, which leads to the reduction
24
25 of Hg^{2+} ions to $\text{Hg}(0)$ atoms by ascorbic acid through the formation of amalgam. The LOD
26
27 obtained using this method was 5.4 nM. This method was successfully applied to the
28
29 determination of Hg^{2+} ions in tap and pond water samples. Heider et al.¹²¹ reported the
30
31 application of thiol-functionalized Au NRs for mercury sensing with high sensitivity. The
32
33 detection of Hg^{2+} ions involved changes in the longitudinal LSPR band through the formation of
34
35 AuHg amalgam in the presence of NaBH_4 . The LOD obtained using this method was $2.28 \times$
36
37 10^{-19} M mercury per NR. This method was successfully applied to the determination of mercury
38
39 in tap water samples.
40
41
42
43
44
45
46
47

48 In general, the blue shift observed in the longitudinal LSPR band is due to the change in
49
50 the dielectric constant of the medium surrounding the Au NRs after the coating of Hg on the
51
52 surface of the Au NRs through the formation of an amalgam, and the effective aspect ratio of the
53
54 NRs is also decreased upon a morphology change. The decrease in the intensity of the
55
56
57
58
59
60

1
2
3 longitudinal LSPR band is due to an increase in the electron density of the Au NRs during the
4
5 formation of the amalgam between the Au and Hg, and thereby affects the plasmonic properties
6
7 of the Au NRs. When the morphology of the NRs changes, their plasmonic properties also
8
9 significantly changes due to the change in the surface geometry.
10
11

12 13 14 **5.2.5. Catalytic etching formation**

15
16 The formation of catalytic etching is also an important sensing mechanism for the
17
18 detection of toxic metal ions. Niu et al.¹²² developed a novel strategy for the colorimetric
19
20 detection of Cu²⁺ ions using Au NRs in the presence of sodium thiosulfate and ammonia. The
21
22 detection of Cu²⁺ ions involved changes in the longitudinal LSPR band by the etching of the Au
23
24 NRs, which induces a decrease in their aspect ratio, and changes in the morphology of Au NRs.
25
26 Moreover, this colorimetric sensor showed high sensitivity and selectivity towards the detection
27
28 of Cu²⁺ ions. The LOD obtained using this method was 1.6 nM. Wang et al.¹²³ developed a novel
29
30 method for the colorimetric detection of Cu²⁺ ions using Au NRs in the presence of H₂O₂ and
31
32 thiocyanate through the decelerating etching of Au NRs. The detection of Cu²⁺ ions involves
33
34 changes in the longitudinal LSPR band *via* catalytic decomposition of H₂O₂ by Cu²⁺ ions, which
35
36 specifically inhibits the corrosion of Au NRs. Moreover, this method showed a sensitive and
37
38 selective detection of Cu²⁺ ions without any other labeling or modification steps. The LOD
39
40 obtained using this method was 4.96 nM. This method was successfully applied to the
41
42 determination of Cu²⁺ ions in shellfish samples. Lan et al.¹²⁴ developed a simple colorimetric
43
44 method for the selective detection of Pb²⁺ ions using Au NRs in the presence of thiosulphate.
45
46 The detection of Pb²⁺ ions involves changes in the longitudinal LSPR band due to the etching of
47
48 Au NRs through the formation of Pd-Au alloy. The LOD obtained using this method was 4.3
49
50 nM. This method was successfully applied to the determination of Pb²⁺ ions in lake, pond,
51
52
53
54
55
56
57
58
59
60

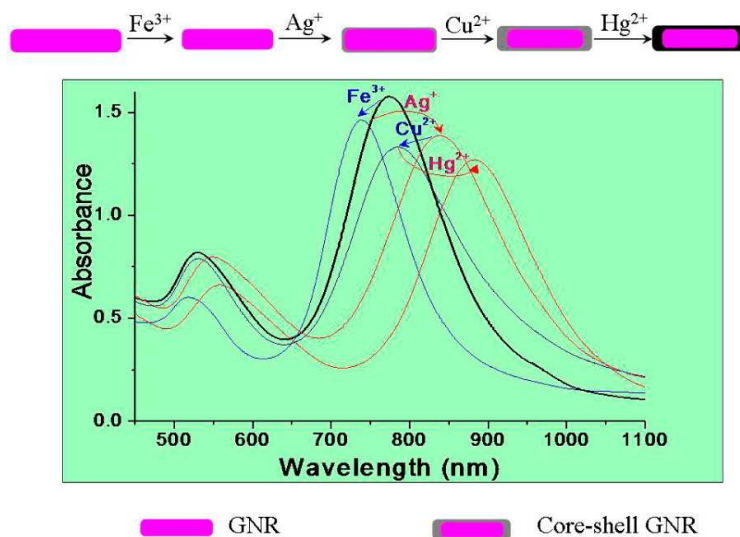
1
2
3 seawater, urine, and soil samples. Chen et al.¹²⁵ developed colorimetric method for the sensing of
4
5 Cu^{2+} ions using Au NRs in an ammonia/ammonium chloride buffer solution containing sodium
6
7 thiosulfate. In this method, the longitudinal LSPR absorption intensity is decreased with a blue
8
9 shift due to the etching of the Au NRs in the presence of dissolved oxygen, along with a color
10
11 change from blue to light red. The LOD obtained using this method was 2.7 nM. This method
12
13 was successfully applied to the determination of Cu^{2+} ions in shellfish samples.
14
15

16 17 18 **5.2.6. Other interactions**

19
20
21 Other than the above types of interactions, the sensing mechanism for the detection of
22
23 toxic metal ions by Au NRs is understood by the agglomeration, chemical redox-mediated inner
24
25 particle interaction, chelation and changes in the structure and composition. Thatai et al.¹²⁶
26
27 developed a sensitive method for the detection of Fe^{3+} ions using Au NRs as a probe. The
28
29 detection of Fe^{3+} ions involved a blue shift in the longitudinal LSPR band of Au NRs through
30
31 agglomeration. The LOD obtained using this method was 0.25 μM (100 ppb). Wang et al.⁹⁰
32
33 reported the colorimetric detection of Hg^{2+} ions using mesoporous silica-coated Au NRs based
34
35 on the mechanism of chemical redox-mediated inner particle interaction. In this method, the
36
37 Hg^{2+} ions are reduced to $\text{Hg}(0)$ in the presence of ascorbic acid and NaBH_4 . Then, the reduced
38
39 $\text{Hg}(0)$ is deposited on the surface of the silica-coated Au NRs with a color change, and the
40
41 addition of S^{2-} to this solution leads to the reverse process due to the extraction of $\text{Hg}(0)$ by S^{2-} .
42
43 The LOD obtained using this method was 0.79 nM. Liu et al.¹²⁷ developed a probe for the
44
45 selective and sensitive detection of Cu^{2+} ions using polyamine-capped Au NRs. Poly(sodium-4-
46
47 styrenesulfonate) and polyethylenimine were electrostatically adsorbed on the positively charged
48
49 CTAB-coated Au NRs using a layer-by-layer self-assembly method. The polyamine-capped Au
50
51 NRs are employed as probes for the detection of Cu^{2+} ions. The longitudinal LSPR band of the
52
53
54
55
56
57
58
59
60

polyamine-capped Au NRs experienced a blue shift due to the specific chelation of the polyethylenimine with Cu^{2+} ions. The LOD obtained using this method was $0.24 \mu\text{M}$. This polyamine-capped Au NR-based LSPR sensor was successfully used for the detection of Cu^{2+} ions in river water.

Huang et al.¹²⁸ developed a label-free multiplex plasmonic sensor for the selective detection of different metal ions, including Fe^{3+} , Hg^{2+} , Cu^{2+} , and Ag^+ ions, based on a single type of Au NRs. The detection of Fe^{3+} , Hg^{2+} , Cu^{2+} , and Ag^+ ions was based on the changes in the longitudinal LSPR band of Au NRs due to the interaction between these metal ions and Au NRs under optimized conditions, which produced changes in the nanostructure and composition of the Au NRs. The detection of Fe^{3+} , Hg^{2+} , Cu^{2+} , and Ag^+ ions and the changes in the longitudinal LSPR band of the NRs, is shown in Fig. 15. This Au NR-based assay is able to successively determine all four kinds of metal ions, along with distinguishing between them. This assay detects Fe^{3+} , Hg^{2+} , Cu^{2+} , and Ag^+ ions with as low as 10^{-6} , 10^{-8} , 10^{-10} , and 10^{-8} M, respectively.



1
2
3 Fig. 15 Schematic illustration of determination of Fe^{3+} , Ag^+ , Cu^{2+} , and Hg^{2+} ions based on a
4 single type of Au NRs. Reproduced with permission from ref. 128 Copyright 2013 The
5 American Chemical Society.
6
7

8 **6. Application for real sample analysis**

9
10 The most important challenge for a Au NR-based sensor is its practical applications to
11 real sample analysis. To validate the practical applicability of a developed sensor method, it
12 should be applied to the determination of the metal ion levels in real samples. Thus, real samples
13 were collected from different nearby sources, e.g., river water, tube well water, drinking water,
14 and industrial effluent water. Initially, the collected water samples were filtered three times
15 through qualitative filter paper to remove any unwanted residue. Then, the collected water
16 samples were checked for the presence of any targeted metal ions. For the real sample analysis, a
17 known concentration of the metal ions was added to the water samples containing the Au NRs
18 probes; the shift in the longitudinal LSPR band due to a change in the surrounding environment
19 after the addition of the metal ions was monitored; and the corresponding shift in the longitudinal
20 LSPR band was analyzed to determine the added metal ion content from the standard addition
21 plot. The standard addition plot was obtained by the addition of known concentrations of metal
22 ions to Au NR-based sensor probes.¹²⁹ By applying the standard addition method, the Au NR-
23 based longitudinal LSPR sensor probes determined the metal ions present in the different water
24 samples with good recovery.
25
26
27
28
29
30
31
32
33
34
35
36
37
38
39
40
41
42
43
44
45

46 Therefore, the developed Au NR-based sensor probes are a convenient means for
47 determining the toxic metal ions present in environmental water samples. From the real sample
48 analysis, the detection of Hg^{2+} ions did not interfere with the real water samples, which indicates
49 that the proposed sensor has potential applications for the detection of the metal ions present in
50 real environmental samples.
51
52
53
54
55
56
57
58
59
60

7. Future Challenges

Although Au NR-based longitudinal LSPR sensing is an effective platform for the detection of toxic metal ions, there are many important challenges still remaining in relation to the modification and application of such Au NR-based sensors. These include improvements in the i) modification of Au NRs, ii) LOD, iii) selectivity toward one particular metal ion in the presence other metal ions, and iv) practical applications. The use of specific functional groups or specific biomolecules for the surface modification of Au NRs is a good example of the improvements made in the modification process and also for good stability. The LOD of Au NR-based longitudinal LSPR sensor system can be improved by the development of modification procedures to prepare modified Au NR probes for the detection of metal ions. The surface functionalization of Au NRs increases the surface absorption capability and fast transport of metal ions toward the surface, which enables the detection of toxic metal ions with enhanced sensitivity. The selectivity of Au NR-based longitudinal LSPR sensor system also requires the effective modification of Au NRs using specific recognition elements as metal ion receptors. Therefore, the development of new sensor designs for the detection of toxic metal ions with more advantages such as high sensitivity, selectivity, fast response time and cost effectiveness by using modified Au NRs is the current field of interest.

Despite these challenges, clearly the unique optical properties of Au NRs and their ability to be easily modified with other materials make them ideal candidates for the detection of toxic metal ions. Au NR-based materials present a good platform for the future development of sensors to detect environmentally toxic metal ions, which could also be extended to environmentally toxic molecules. As a result, Au NR-based LSPR sensor will be a versatile method for the detection of metal ions in the near future.

8. Conclusions

The unique optical properties of Au NRs make them an attractive platform for the detection of metal ions based on the longitudinal LSPR band of the Au NRs. The effective surface modification of Au NRs shows improved selectivity and sensitivity in the detection of toxic metal ions. Different methods are discussed for the preparation of surface-modified Au NRs for the detection of toxic metal ions based on the longitudinal LSPR band of the Au NRs, along with the types of interactions between the surface of the NRs and metal ions. In this review article, we have broadly summarized various strategies that have been implemented for the design of chemical interactions between metal ions and the surface of Au NRs. Surface functionalized Au NRs act as both recognition elements for binding with metal ions and transducers for signaling, which simplifies the design of a sensor with improved sensitivity and selectivity. The surface modification of Au NRs with functional groups will introduce a new direction in the field of sensor design. Most of the reported Au NR-based longitudinal LSPR sensors showed lower detection limit for detection of toxic metals ions than the permissible limits of such toxic metal ions and relative to the AAS, ICP-MS, and electrochemical techniques for detection of metal ions, the Au NR-based longitudinal LSPR sensors shows comparable LODs, less time consuming, and low cost instrumentation is sufficient. Although the unique properties of Au NRs have offered many advantages for the detection of environmentally toxic metal ions, further efforts should be made by focusing on the development of an effective modification of Au NRs to improve their biocompatible, long-term stability, and specific binding with metal ions for the fabrication of sensor systems with enhanced sensitivity and selectivity. Their applications should also be extended to validate their use in real sample analysis. The chemical functionalization of Au NRs with polymers, biomaterials, or silica-based materials

allows for the fabrication of a diverse range of metal ion sensors that could be tailored using various kinds of coatings on the surface of the NRs in order to improve the analytical metal ion detection performance. The Au NR-based longitudinal LSPR sensor is a versatile method for the detection of toxic metal ions in future.

Acknowledgement

The authors wish to express their gratitude to the Ministry of Higher Education and the University of Malaya for sanctioning a High Impact Research Grant (UM.C/625/1/HIR/MOHE/SC/21) and UMRG Programme Grant (RP007C/13AFR).

References

- 1 X. Huang, S. Neretina and M. A. El-Sayed, *Adv. Mater.*, 2009, **21**, 4880.
- 2 J. Perez-Juste, I. Pastoriza-Santos, L. M. Liz-Marzan and P. Mulvaney, *Coord. Chem. Rev.*, 2005, **249**, 1870.
- 3 H. Chen, L. Shao, Q. Li and J. Wang, *Chem. Soc. Rev.*, 2013, **42**, 2679.
- 4 T. K. Sau, A. L. Rogach, F. Jackel, T. A. Klar and J. Feldmann, *Adv. Mater.*, 2010, **22**, 1805.
- 5 V. Sharma, K. Park and M. Srinivasarao, *Mater. Sci. Eng. R-Rep.*, 2009, **65**, 1.
- 6 J. Cao, E. K. Galbraith, T. Sun and K. T. Grattan, *Sens. Actuators, B*, 2012, **169**, 360.
- 7 C. Wang, Z. Ma, T. Wang and Z. Su, *Adv. Funct. Mater.*, 2006, **16**, 1673.
- 8 S. Link, M. B. Mohamed and M. A. El-Sayed, *J. Phys. Chem. B*, 1999, **103**, 3073.
- 9 A. M. Alkilany, L. B. Thompson, S. P. Boulos, P. N. Sisco and C. J. Murphy, *Adv. Drug Deliv. Rev.*, 2012, **64**, 190.

- 1
2
3
4
5
6
7
8
9
10
11
12
13
14
15
16
17
18
19
20
21
22
23
24
25
26
27
28
29
30
31
32
33
34
35
36
37
38
39
40
41
42
43
44
45
46
47
48
49
50
51
52
53
54
55
56
57
58
59
60
- 10 P. K. Jain, X. Huang, I. H. El-Sayed and M. A. El-Sayed, *Acc. Chem. Res.*, 2008, **41**, 1578.
- 11 W. -S. Kuo, C. -N. Chang, Y. -T. Chang, M. -H. Yang, Y. -H. Chien, S. -J. Chen and C. -S. Yeh, *Angew. Chem. Int. Ed.*, 2010, **49**, 2711.
- 12 X. Huang, I. H. El-Sayed, W. Qian and M. A. El-Sayed, *J. Am. Chem. Soc.*, 2006, **128**, 2115.
- 13 S. A. El-Safty, M. A. Shenashen and S. A. El-Safty, *Trends Anal. Chem.*, 2012, **38**, 98.
- 14 C. McDonagh, C. S. Burke and B. D. MacCraith, *Chem. Rev.*, 2008, **108**, 400.
- 15 N. J. Ronkainen, H. B. Halsall and W. R. Heineman, *Chem. Soc. Rev.*, 2010, **39**, 1747.
- 16 S. Nagl and O. S. Wolfbeis, *Analyst*, 2007, **132**, 507.
- 17 K. Kalantar-zadeh and B. Fry, *Nanotechnology-Enabled Sensors*, Springer Science+Business Media, New York, USA, 2008.
- 18 K. Saha, S. S. Agasti, C. Kim, X. Li and V. M. Rotello, *Chem. Rev.*, 2012, **112**, 2739.
- 19 J. Homola, *Chem. Rev.*, 2008, **108**, 462.
- 20 H. N. Kim, W. X. Ren, J. S. Kim and J. Yoon, *Chem. Soc. Rev.*, 2012, **41**, 3210.
- 21 L. Chen, X. Fu, W. Lu and L. Chen, *ACS Appl. Mater. Interfaces*, 2013, **5**, 284.
- 22 T. Lou, Z. Chen, Y. Wang and L. Chen, *ACS Appl. Mater. Interfaces*, 2011, **3**, 1568.
- 23 J. M. Slocik, J. S. Zabinski, D. M. Phillips and R. R. Naik, *Small*, 2008, **4**, 548.
- 24 J. H. Duffus, *Pure Appl. Chem.*, 2002, **74**, 793.
- 25 G. Aragay, J. Pons and A. Merkoçi, *Chem. Rev.*, 2011, **111**, 3433.
- 26 Y. Lou, Y. Zhao, J. Chen and J. J. Zhu, *J. Mater. Chem. C*, 2014, **2**, 595.
- 27 Y. W. Lin, C. C. Huang and H. T. Chang, *Analyst*, 2011, **136**, 863.

- 1
2
3 28 S. J. Lee, J. –E. Lee, J. Seo, Y. Jeong, S. S. Lee and J. H. Jung, *Adv. Funct. Mater.*, 2007,
4 17, 3441.
5
6
7
8 29 S. J. Stohs and D. Bagchi, *Free Radic. Biol. Med.*, 1995, **18**, 321.
9
10 30 F. Fu and Q. Wang, *J. Environ. Manage.*, 2011, **92**, 407.
11
12 31 D. H. Nies, *Appl. Microbiol. Biotechnol.*, 1999, **51**, 730.
13
14 32 K. E. Giller, E. Witter and S. P. Mcgrath, *Soil Biol. Biochem.*, 1998, **30**, 1389.
15
16 33 World Health Organization, Guidelines for drinking-water quality, 3rd ed., vol. 1,
17 Geneva, 2004, 188.
18
19
20 34 L. Vigderman, B. P. Khanal and E. R. Zubarev, *Adv. Mater.*, 2012, **24**, 4811.
21
22 35 T. Placido, G. Aragay, J. Pons, R. Comparelli, M. L. Curri and A. Merkoci, *ACS Appl.*
23 *Mater. Interfaces*, 2013, **5**, 1084.
24
25
26 36 S. Eustis and M. A. El-Sayed, *Chem. Soc. Rev.*, 2006, **35**, 209.
27
28 37 C. M. Cobley, J. Chen, E. C. Cho, L. V. Wang and Y. Xia, *Chem. Soc. Rev.*, 2011, **40**, 44.
29
30 38 S. K. Ghosh and T. Pal, *Chem. Rev.*, 2007, **107**, 4797.
31
32 39 K. G. Thomas, Current Trends in Science, Platinum Jubilee Special, 2009, 53.
33
34 40 L. Tong, Q. Wei, A. Wei and J. X. Cheng, *Photochem. Photobiol.*, 2009, **85**, 21.
35
36 41 E. Hutter and J. H. Fendler, *Adv. Mater.*, 2004, **16**, 1685.
37
38 42 K. A. Willets and R. P. Van Duyne, *Annu. Rev. Phys. Chem.*, 2007, **58**, 267.
39
40 43 C. J. Murphy, A. M. Gole, S. E. Hunyadi, J. W. Stone, P. N. Sisco, A. Alkilany and P.
41 Hankins, *Chem. Commun.*, 2008, **5**, 544.
42
43
44 44 K. L. Kelly, E. Coronado, L. L. Zhao and G. C. Schatz, *J. Phys. Chem. B*, 2003, **107**, 668.
45
46 45 K. S. Lee and M. A. El-Sayed, *J. Phys. Chem. B*, 2006, **110**, 19220.
47
48
49
50
51
52
53
54
55
56
57
58
59
60

- 1
2
3
4 46 M. A. Mackey, M. R. K. Ali, L. A. Austin, R. D. Near and M. A. El-Sayed, *J. Phys.*
5
6 *Chem. B*, 2014, **118**, 1319.
7
8 47 M. N'Gom, S. Li, G. Schatz, R. Erni, A. Agarwal, N. Kotov and T. B. Norris, *Phys. Rev.*
9
10 *B*, 2008, **80**, 113411.
11
12 48 B. Nikoobakht and M. A. El-Sayed, *Chem. Mater.*, 2003, **15**, 1957.
13
14 49 N. R. Jana, L. Gearheart and C. J. Murphy, *J. Phys. Chem. B*, 2001, **105**, 4065.
15
16 50 A. Gole and C. J. Murphy, *Chem. Mater.*, 2004, **16**, 3633.
17
18 51 S. E. Lohse and C. J. Murphy, *Chem. Mater.*, 2013, **25**, 1250.
19
20 52 X. C. Ye, L. H. Jin, H. Caglayan, J. Chen, G. Z. Xing, C. Zheng, V. Doan-Nguyen, Y. J.
21
22 Kang, N. Engheta, C. R. Kagan and C. B. Murray, *ACS Nano*, 2012, **6**, 2804.
23
24 53 Y.-Y. Yu, S.-S. Chang, C.-L. Lee and C. R. C. Wang, *J. Phys. Chem. B*, 1997, **101**, 6661.
25
26 54 K. Okitsu, K. Sharyo and R. Nishimura, *Langmuir*, 2009, **25**, 7786.
27
28 55 F. Kim, J. H. Song and P. D. Yang, *J. Am. Chem. Soc.*, 2002, **124**, 14316.
29
30 56 J. M. Cao, X. J. Ma, M. B. Zheng, J. S. Liu and H. M. Ji, *Chem. Lett.*, 2005, 730.
31
32 57 Y.-J. Zhu and X.-L. Hu, *Chem. Lett.*, 2003, 1140.
33
34 58 J.-S. Huang, V. Callegari, P. Geisler, C. Brüning, J. Kern, J. C. Prangma, X. F. Wu, T.
35
36 Feichtner, J. Ziegler, P. Weinmann, M. Kamp, A. Forchel, P. Biagioni, U. Sennhauser
37
38 and B. Hecht, *Nat. Commun.*, 2010, **1**, 150.
39
40 59 P. B. Dayal and F. Koyama, *Appl. Phys. Lett.*, 2007, **91**, 111107.
41
42 60 H. Petrova, J. Perez-Juste, Z. Zhang, J. Zhang, T. Kosel and G. V. Hartland, *J. Mater.*
43
44 *Chem.*, 2006, **16**, 3957.
45
46 61 A. M. Alkilany, P. K. Nagaria, C. R. Hexel, T. J. Shaw, C. J. Murphy and M. D. Wyatt,
47
48 *Small*, 2009, **5**, 701.
49
50
51
52
53
54
55
56
57
58
59
60

- 1
2
3
4 62 C. Kinnear, H. Dietsch, M. J. D. Clift, C. Endes, B. Rothen-Rutishauser and A. Petri-
5 Fink, *Angew. Chem. Int. Ed.*, 2013, **52**, 1934.
6
7
8 63 T. S. Hauck, A. A. Ghazani and W. C. W. Chan, *Small*, 2008, **4**, 153.
9
10 64 C. J. Murphy, L. B. Thompson, A. M. Alkilany, P. N. Sisco, S. P. Boulos, S. T.
11 Sivapalan and J. Huang, *J. Phys. Chem. Lett.*, 2010, **1**, 2867.
12
13
14 65 C. Gui and D. Cui, *Cancer Biol. Med.*, 2012, **9**, 221.
15
16
17 66 B. Thierry, J. Ng, T. Krieg and H. J. Griesser, *Chem. Commun.*, 2009, **13**, 1724.
18
19
20 67 C. Yu, L. Varghese and J. Irudayaraj, *Langmuir*, 2007, **23**, 9114.
21
22 68 A. Wijaya and K. Hamad-Schifferli, *Langmuir*, 2008, **24**, 9966.
23
24
25 69 S. Y. Hwang, A. R. Tao, *Pure Appl. Chem.*, 2010, **83**, 233.
26
27 70 J. Cao, E. K. Galbraith, T. Sun and K. T. Grattan, *Sens. Actuators, B*, 2012, **169**, 360.
28
29 71 Z. Ma, H. Xia, Y. Liu, B. Liu, W. Chen and Y. Zhao, *Chin. Sci. Bull.*, 2013, **58**, 2530.
30
31 72 Z. Zhang, J. Wang and C. Chen, *Theranostics*, 2013, **3**, 223.
32
33
34 73 E. T. Castellana, R. C. Gamez, M. E. Gomez and D. H. Russell, *Langmuir*, 2010, **26**,
35 6066.
36
37
38 74 V. Biju, *Chem. Soc. Rev.*, 2014, **43**, 744.
39
40
41 75 I. Willner and B. Willner, *Nano Lett.*, 2010, **10**, 3805.
42
43
44 76 R. Mout, D. F. Moyano, S. Rana and V. M. Rotello, *Chem. Soc. Rev.*, 2012, **41**, 2539.
45
46 77 H. Ju, X. Zhang and J. Wang, *NanoBiosensing: Principles, Development and*
47 *Application*, Springer Science+Business Media, New York, USA, 2011.
48
49
50 78 H. Takahashi, Y. Niidome, T. Niidome, K. Kaneko, H. Kawasaki and S. Yamada,
51 *Langmuir*, 2006, **22**, 2.
52
53
54
55 79 Q. Dai, J. Coutts, J. Zou and Q. Huo, *Chem. Commun.*, 2008, 2858.
56
57
58
59
60

- 1
2
3
4 80 A. Gole and C. J. Murphy, *Chem. Mater.*, 2005, **17**, 1325.
5
6 81 H. Takahashi, T. Niidome, T. Kawano, S. Yamada and Y. Niidome, *J. Nanopart. Res.*,
7
8 2008, **10**, 221.
9
10 82 J. W. Hotchkiss, A. B. Lowe and S. G. Boyes, *Chem. Mater.*, 2007, **19**, 6.
11
12 83 S. Liu and M. -Y. Han, *Chem. Asian J.*, 2010, **5**, 36.
13
14 84 S. Jayabal and R. Ramaraj, *Electrochim. Acta*, 2013, **88**, 51.
15
16 85 C. Wu and Q.-H. Xu, *Langmuir*, 2009, **25**, 9441.
17
18 86 I. E. Sendroiu, M. E. Warner and R. M. Corn, *Langmuir*, 2009, **25**, 11282.
19
20 87 G. Wang, Z. Chen and L. Chen, *Nanoscale*, 2011, **3**, 1756.
21
22 88 S. Jayabal, P. Viswanathan and R. Ramaraj, *RSC Adv.*, 2014, **4**, 33541.
23
24 89 Z. Zhang, L. Wang, J. Wang, X. Jiang, X. Li, Z. Hu, Y. Ji, X. Wu and C. Chen, *Adv.*
25
26 *Mater.*, 2012, **24**, 1418.
27
28 90 G. Wang, Z. Chen, W. Wang, B. Yan and L. Chen, *Analyst*, 2011, **136**, 174.
29
30 91 L. Polavarapu, J. Perez-Juste, Q. -H. Xu and L. M. Liz-Marzan, *J. Mater. Chem. C*, 2014,
31
32 **2**, 7460.
33
34 92 H. Xu, Y. Wang, X. Huang, Y. Li, H. Zhang and X. Zhong, *Analyst*, 2012, **137**, 924.
35
36 93 Y. Si, X. Wang, Y. Li, K. Chen, J. Wang, J. Yu, H. Wang and B. Ding, *J. Mater. Chem.*
37
38 *A*, 2014, **2**, 645.
39
40 94 K. Farhadi, M. Forough, R. Molaei, S. Hajizadeh and A. Rafipour, *Sens. Actuators B*,
41
42 2012, **161**, 880.
43
44 95 C. -Y. Lin, C. -J. Yu, Y. -H. Lin and W. -L. Tseng, *Anal. Chem.*, 2010, **82**, 6830.
45
46 96 T. Placido, G. Aragay, J. Pons, R. Comparelli, M. L. Curri and A. Merkoci, *ACS Appl.*
47
48 *Mater. Interfaces*, 2013, **5**, 1084.
49
50
51
52
53
54
55
56
57
58
59
60

- 1
2
3 97 S. Jayabal, R. Sathiyamurthi and R. Ramaraj, *J. Mater. Chem. A*, 2014, **2**, 8918.
4
5 98 G. Chen, Y. Jin, L. Wang, J. Deng and C. Zhang, *Chem. Commun.*, 2011, **47**, 12500.
6
7
8 99 Y. He, J. Tian, J. Zhang, S. Chen, Y. Jiang, K. Hu, Y. Zhao, S. Zhao, *Biosens.*
9
10 *Bioelectron.*, 2014, **55**, 285.
11
12 100 C. Jing, L. Shi, X. Liu and Y. -T. Long, *Analyst*, 2014, **139**, 6435.
13
14 101 Y. Zhu, L. Xu, W. Ma, Z. Xu, H. Kuang, L. Wang and C. Xu, *Chem. Commun.*, 2012, **48**,
15 11889.
16
17
18 102 S. Chen, D. Liu, Z. Wang, X. Sun, D. Cui and X. Chen, *Nanoscale*, 2013, **5**, 6731.
19
20 103 R. Puk and J. H. Weber, *Anal. Chim. Acta*, 1994, **292**, 175.
21
22 104 Y. Li, C. Chen, B. Li, J. Sun, J. Wang, Y. Gao, Y. Zhao and Z. Chai, *J. Anal. At.*
23 *Spectrom.*, 2006, **21**, 94.
24
25
26 105 M. B. Gholivand and M. H. Parvin, *Electroanalysis*, 2010, **22**, 2291.
27
28 106 A. Klinkova, R. M. Choueiri and E. Kumacheva, *Chem. Soc. Rev.*, 2014, **43**, 3976.
29
30 107 P. R. Sajanlal, T. S. Sreeprasad, A. K. Samal and T. Pradeep, *Nano Rev.*, 2011, **2**, 5883.
31
32 108 B. Goris, S. Bals, W. Van den Broek, E. Carbó-Argibay, S. Gómez-Graña, L. M. Liz-
33 Marzán and G. V. Tendeloo¹, *Nat. Mater.*, 2012, **11**, 930.
34
35 109 E. Carbo-Argibay, B. Rodríguez-Gonzalez, I. Pastoriza-Santos, J. Perez-Juste and L. M.
36 Liz-Marzan, *Nanoscale*, 2010, **2**, 2377.
37
38
39 110 O. A. Oviedo, E. P. M. Leiva and M. M. Mariscal, *Phys. Chem. Chem. Phys.*, 2008, **10**,
40 3561.
41
42
43 111 S. -Y. Zhang, M. D. Regulacio and M. -Y. Han, *Chem. Soc. Rev.*, 2014, **43**, 2301.
44
45 112 P. K. Jain, S. Eustis and M. A. El-Sayed, *J. Phys. Chem. B*, 2006, **110**, 18243.
46
47
48
49
50
51
52
53
54
55
56
57
58
59
60

- 1
2
3
4
5
6
7
8
9
10
11
12
13
14
15
16
17
18
19
20
21
22
23
24
25
26
27
28
29
30
31
32
33
34
35
36
37
38
39
40
41
42
43
44
45
46
47
48
49
50
51
52
53
54
55
56
57
58
59
60
- 113 P. R. Selvakannan, E. Dumas, F. Dumur, C. P  choux, P. Beaunier, A. Etcheberry and C. R. Mayer, *J. Colloid Interface Sci.*, 2010, **349**, 93.
- 114 J. -M. Liu, H. -F. Wang and X. -P. Yan, *Analyst*, 2011, **136**, 3904.
- 115 H. H. Cai, D. Lin, J. Wang, P. H. Yang and J. Cai, *Sens. Actuators, B*, 2014, **196**, 252.
- 116 N. Bi, Y. Chen, H. Qi, X. Zheng, Y. Chen, X. Liao, H. Zhang and Y. Tian, *Sens. Actuators B*, 2012, **166–167**, 766.
- 117 G. Chen, Y. Jin, W. Wang and Y. Zhao, *Gold Bull.*, 2012, **45**, 137.
- 118 M. Rex, F. E. Hernandez and A. D. Campiglia, *Anal. Chem.*, 2006, **78**, 445.
- 119 W. Chemnasiri and F. E. Hernandez, *Sens. Actuators B*, 2012, **173**, 322.
- 120 G. S. Anand, A. I. Gopalan, S. -W. Kang and K. -P. Lee, *J. Anal. At. Spectrom.*, 2013, **28**, 488.
- 121 E. C. Heider, K. Trieu, A. F. Moore and A. D. Campiglia, *Talanta*, 2012, **99**, 180.
- 122 X. Niu, D. Xu, Y. Yang and Y. He, *Analyst*, 2014, **139**, 2691.
- 123 S Wang, Z. Chen, L. Chen, R. Liu and L. Chen, *Analyst*, 2013, **138**, 2080.
- 124 Y. -J. Lan, and Y. -W. Lin, *Anal. Methods*, 2014, **6**, 7234.
- 125 Z. Chen, R. Liu, S. Wang, C. Qu, L. Chena and Z. Wang, *RSC Adv.*, 2013, **3**, 13318.
- 126 S. Thatai, P. Khurana, S. Prasad and D. Kumar, *Microchem. J.*, 2014, **113**, 77.
- 127 Y. Liu, Y. Zhao, Y. Wang and C. M. Li, *J. Colloid Interface Sci.*, 2015, **439**, 7.
- 128 H. Huang, S. Chen, F. Liu, Q. Zhao, B. Liao, S. Yi, and Y. Zeng, *Anal. Chem.*, 2013, **85**, 2312.
- 129 J. Xue, P. T. Lee and R. G. Compton, *Electroanalysis*, 2014, **26**, 1454.